

Carson Pass–Kirkwood paleocanyon system: Paleogeography of the ancestral Cascades arc and implications for landscape evolution of the Sierra Nevada (California)

C.J. Busby[†]

S.B. DeOreo

Department of Earth Science, University of California, Santa Barbara, California 93101, USA

I. Skilling

Department of Geology and Planetary Sciences, University of Pittsburgh, 200 SRCC, Pittsburgh, Pennsylvania 15260, USA

P.B. Gans

Department of Earth Science, University of California, Santa Barbara, California 93101, USA

J.C. Hagan

Department of Earth Science, University of California, Santa Barbara, California 93101, USA

ABSTRACT

Tertiary strata of the central Sierra Nevada are dominated by widespread, voluminous volcanic breccias that are largely undivided and undated, the origin of which is poorly understood. These dominantly andesitic strata are interpreted to be eruptive products of the ancestral Cascades arc, deposited and preserved within paleocanyons that crossed the present-day Sierra Nevada before Basin and Range faulting began there. These strata are thus important not only for understanding the paleogeography of the Ancestral Cascades arc, but also for reconstructing the evolution of the Sierra Nevada landscape.

Our regional-scale mapping shows that paleocanyon fills of the central Sierra Nevada are dominated by intrusions and vent-proximal facies along the present-day Sierran crest, with more distal facies extending westward down the paleocanyons. Vent-proximal facies consist of lava domes that collapsed to generate block and ash flow tuffs, which in turn were remobilized down-canyon to produce coarse-grained volcanic mudflow and dilute flow (fluvial) deposits. Lava flows are rare; instead, magmas invaded wet volcanoclastic sediment to form *in situ* peperite piles that were partly remobilized to form debris flows or block and ash flows with peperite domains.

Detailed mapping and dating of previously undifferentiated Tertiary strata in the

Carson Pass–Kirkwood area of the central Sierra Nevada has allowed us to identify 6 unconformity-bounded sequences preserved within a paleocanyon as deep as 650 m cut into Mesozoic granitic basement. The Carson Pass–Kirkwood paleocanyon trends NE–SW, with a paleo-transport direction roughly parallel to the modern Mokelumne River drainage (toward the SW). Sequence 1 consists of Oligocene silicic ignimbrites sourced from Nevada. Sequences 2 through 6 consist of dominantly andesitic rocks of the Miocene Ancestral Cascades arc, with ⁴⁰Ar/³⁹Ar ages ranging from 14.69 ± 0.06 Ma to 6.05 ± 0.12 Ma. These new dates provide constraints on the ages of unconformities.

Vertical relief on the unconformities within the paleocanyon ranges from 12 to 303 meters; with paleoslope gradients range from 3° to 48°. No evidence exists for widening or deepening of the paleocanyon into Mesozoic basement during Tertiary time, so we infer that unconformity 1 (the paleocanyon floor and walls) was inherited from Cretaceous time. The deepest unconformities within the paleocanyon fill reincised into granitic basement in the early Miocene (unconformity 2), between 14 and 10 Ma (unconformity 5), and between 10 and 6 Ma (unconformity 6). The paleocanyon was also beheaded (cut off from sources to the east) by ca. 10 Ma. We suggest that the early Miocene reincision records tectonism related to the onset of arc magmatism in the Sierra Nevada. The middle Miocene reincision may record the onset of Basin and

Range faulting in the central Sierra. The late Miocene reincision may correspond to uplift attendant with the northward sweep of the triple junction through the latitude of the central Sierra. Paleocanyons of the central Sierra differ from those of the northern and southern Sierra by showing steeper local paleorelief, and the bouldery stream deposits attest to higher axial gradients than envisioned for other parts of the range. This may indicate that the uplift history of the range is not uniform from segment to segment.

Keywords: Sierra Nevada, ancestral Cascades arc, Miocene volcanism, landscape evolution, Basin and Range.

INTRODUCTION

Volcanic and volcanoclastic rocks cover much of the northern and central Sierra Nevada, California, and represent a piece of the Miocene volcanic-tectonic puzzle relative to the rest of the western United States. Filling this gap in our knowledge is important because the Miocene was a time of fundamental tectonic change (Fig. 1A; Atwater, 1970; Dickinson, 1997). The Miocene missing piece of the volcanic-tectonic puzzle is important because it is surrounded by and potentially influenced by any combination of the following events: hotspot magmatism, Cascadian subduction and triple junction migration, Basin and Range extension, and Sierran root delamination (Fig. 1A; McKee and Noble, 1976; Ducea and Saleeby, 1996; Garrison et al., 2007).

[†]busby@geol.ucsb.edu

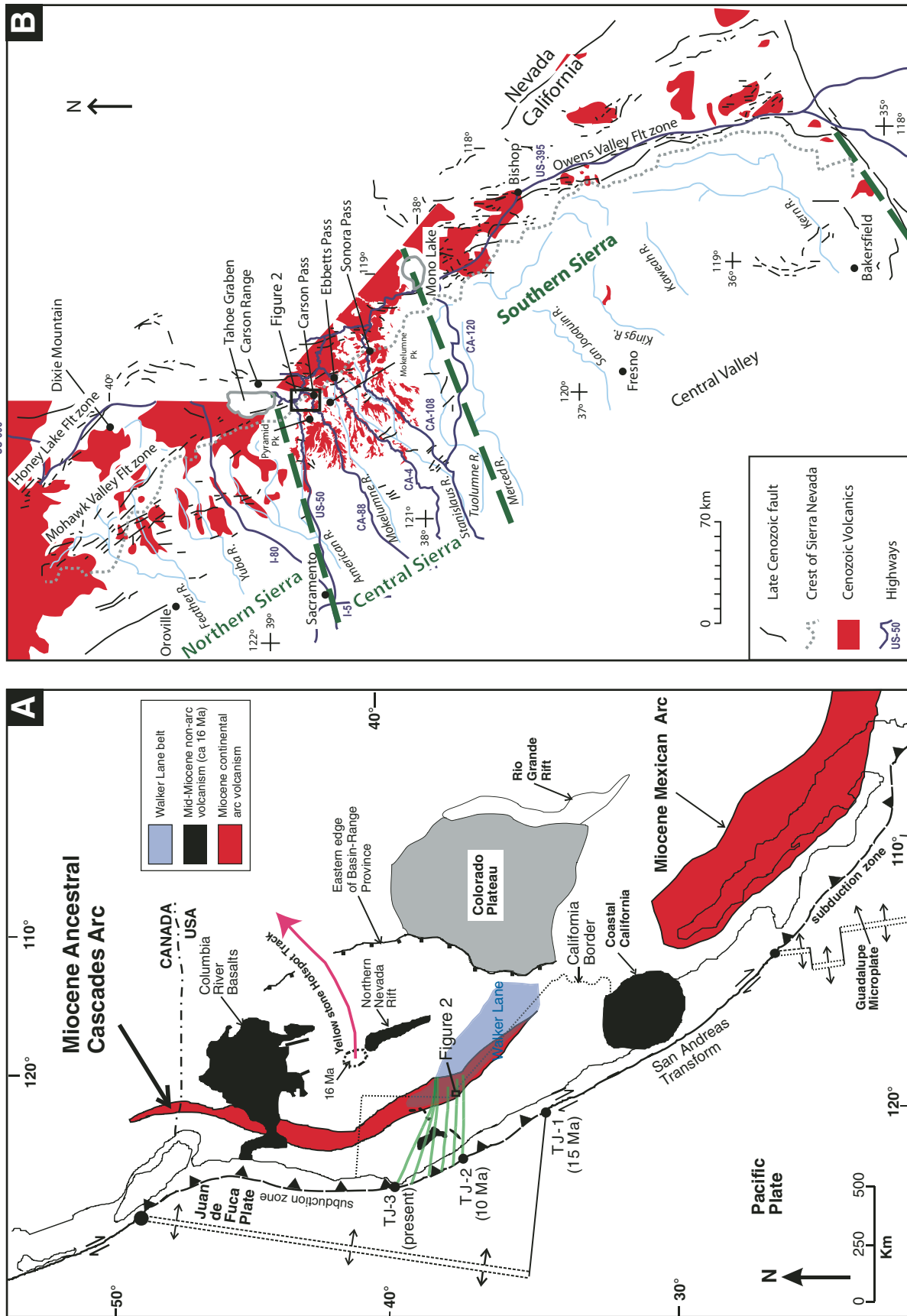


Figure 1. (A) Miocene tectonic elements and magmatic provinces, modified after Dickinson (1997). The Carson Pass–Kirkwood Valley area (Fig. 2) is within the ancestral Cascades arc at the present-day crest of the Sierra Nevada and along the western edge of the Walker Lane. T-J-1, T-J-2, T-J-3 are inferred positions of triple junction through time. (B) Cenozoic volcanic rocks, faults, and geographic features of the Sierra Nevada and adjacent easternmost California. The crest of this highly asymmetric range is very close to the Sierra Nevada frontal fault system (faults taken from Wakabayashi and Sawyer, 2001). Cenozoic volcanic rocks and intrusions are very sparse in the southern Sierra. Cenozoic volcanic-volcaniclastic strata are largely preserved within paleochannels in the central and northern Sierra; we point out geologic differences between the central and northern Sierra in the text. The area mapped in Figure 2, as well as other central Sierran localities discussed in the text, are shown here. Green dashed lines indicate our usage of subdivisions between “northern,” “central,” and “southern” Sierra Nevada (labeled in green letters).

North Fork Mokelumne River (Fig. 1B). Rocks of the Carson Pass–Kirkwood paleocanyon were previously undivided, despite the fact that they are extremely well exposed and easily accessible. We divide the voluminous breccias and paleocanyon fill into mappable lithofacies, which we interpret in terms of arc paleogeography and volcano-sedimentary processes (Table 1). We then use our lithofacies mapping to demonstrate that the paleocanyon fill is divided by at least six erosional unconformities (Figs. 2, 3, and 4). These represent Sierran paleocanyon reincision events not recognized prior to our study. We provide age constraints on the canyon fill and its unconformities by presenting new $^{40}\text{Ar}/^{39}\text{Ar}$ on the volcanic and intrusive rocks. We then use these data to make inferences about the evolution of the central Sierra Nevada landscape.

LITHOFACIES AND UNCONFORMITIES

The oldest paleocanyon fill deposits in the Carson Pass–Kirkwood area, as well as other paleocanyons of the central Sierra (Slemmons, 1953), consist of nonwelded to welded rhyolite ignimbrites (Fig. 2; Table 1). We infer that these are correlative with Oligocene–early Miocene (ca. 20–34 Ma) rhyolite tuffs referred to as the Delleker Formation in the northern Sierra Nevada, and the Valley Springs Formation in the central Sierra (Wagner et al., 1981; Saucedo and Wagner, 1992). Ignimbrites of the northern Sierra form thick stratigraphic successions with numerous ignimbrites, making it possible to correlate them with source calderas in central Nevada (Davis et al., 2000; Hinz et al., 2003; Henry et al., 2003; Faulds et al., 2005a; Garside et al., 2005). Ignimbrites of the central Sierra Nevada, in contrast, were deeply eroded in the early Miocene (as discussed in the following), so it may not be possible to make such detailed correlations.

The Carson Pass–Kirkwood paleocanyon fill is dominated by intermediate-composition fragmental volcanic and volcanoclastic rocks (Fig. 2). These form part of the Miocene Merhten Formation of the central and northern Sierra Nevada (Piper et al., 1939; Curtis, 1951, 1954; Wagner and Saucedo, 1990; Saucedo and Wagner, 1992).

UNCONFORMITIES

The Carson Pass–Kirkwood paleocanyon fill is divided by erosional unconformities that form mappable surfaces that truncate underlying map units (Figs. 2, 3, and 4). Accordingly, the stratigraphy is divided into six unconformity-bounded sequences, each sequence numbered to correspond to the unconformity that underlies

it (Fig. 2B). We use unconformity surfaces as sequence boundaries without specifying a mechanism for their formation (e.g., Pekar et al., 2003; Bassett and Busby, 2007), such as tectonics, base-level change, or climate change.

Preserved vertical relief on the unconformities ranges from 12 to 650 m, and paleoslope gradients on the unconformity surfaces range from 3° to 70° (Fig. 3). No faults occur in the map area (Fig. 2). Therefore, the steep slopes of these unconformities represent the original gradients on these depositional surfaces (minus the effect of regional 1.8° – 2.5° westward tilting of the Sierra Nevada; Unruh, 1991). These unconformity surfaces thus record Cenozoic paleorelief in the Carson Pass–Kirkwood area. Other than the basal unconformity, a nonconformity between Mesozoic bedrock and Tertiary strata (unconformity 1), the deepest unconformities are the youngest ones, with unconformities 5 and 6 locally cutting through all older sequences down to granitic basement.

LITHOFACIES

The volcanic-volcanoclastic terminology used in this paper largely follows that of Fisher and Schminke (1984), Heiken and Wohletz (1985), and Sigurdsson et al. (2000). Lithofacies names are assigned based on compositions, depositional structures and textures, and inferred volcanic or sedimentary eruptive and depositional processes (Table 1). Previous workers largely divided andesites of the area into intrusions and strata, in places incorrectly, and most of the andesitic strata were lumped together as breccias. In this section we show how these so-called breccias can be divided into several mappable lithofacies, which can then be used to reconstruct the paleogeography and structure of the region.

Lithofacies in the Carson Pass–Kirkwood paleocanyon include nonfragmental rocks, interpreted as intrusions and flows; monolithic fragmental rocks, interpreted as flow breccias and block and ash flow tuffs; and polyolithic andesite fragmental rocks, interpreted as debris-flow and streamflow deposits. These lithofacies interfinger laterally and repeat vertically (Fig. 2), so they cannot be described in order of relative age. Instead, we describe them in order of inferred vent-proximal to vent-distal settings; we then describe basalt lava flows, which are volumetrically minor, followed by a description of *in situ* and resedimented peperites.

Intrusions

Intrusions are easiest to recognize when they are large, coherent (i.e., nonfragmental) bodies, with no internal stratification; cliff and bench topography may be mistaken for flow

stratigraphy, when closer examination shows it to be a single massive intrusion. Intrusions within the Carson Pass–Kirkwood paleocanyon commonly pass upward into lava-dome breccias that interfinger with block and ash flow deposits or volcanic debris-flow deposits. Alternatively, intrusions form complex contacts with enclosing volcanoclastic sediment, described as *in situ* and resedimented peperite.

Block and Ash Flow Tuffs

Block and ash flow tuffs are small-volume pyroclastic flow deposits characterized by a large fraction of dense to moderately vesicular juvenile blocks in a massive, unsorted, medium to coarse ash matrix of the same composition (Fig. 5A). They show evidence for hot emplacement, including bread-crust bombs, prismatically jointed blocks, and plastically deformed clasts (Fisher and Schminke, 1984; Freundt et al., 2000; Miyabuchi, 1999). Eruption mechanisms for block and ash flows include gravitational or explosive collapse of lava domes (Fisher and Heiken, 1982; Camus et al., 2000; Voight et al., 2000) or (explosive) Vulcanian eruption columns (Fisher et al., 1980; Freundt et al., 2000). We find no evidence for explosive volcanism at Carson Pass in the form of pumiceous and/or scoriaceous flow deposits, and pyroclastic fall or surge deposits are also lacking. Instead, the block and ash flow tuffs can in places be traced directly into dome breccias. We therefore infer that fragmentation was accomplished by lava-dome collapse, in some cases augmented by magma-wet sediment interaction (Skilling et al., 2004.), described as peperites.

Volcanic Debris-Flow Deposits and Streamflow Deposits

Volcanic debris-flow deposits are thick-bedded to very thick bedded, unsorted deposits of angular to subangular clasts set in a pebbly sandstone matrix (Fig. 5B). They are generally distinguished from block and ash flow deposits at a distance by their color (brown instead of dark gray) and their lesser resistance to weathering. Blocks in the debris-flow deposits may be monolithic or polyolithic, but the matrix is polyolithic, composed of numerous volcanic rock fragment types. Debris-flow deposits do not contain prismatically jointed blocks or bread-crust bombs, which are too fragile to survive resedimentation (Fisher and Schminke, 1984). Debris-flow deposits may also pass upward or laterally into hyperconcentrated flood-flow deposits, which commonly exhibit crude stratification and inverse to normal grading (Fig. 5C).

Streamflow deposits are well-stratified, relatively well-sorted clast-supported deposits composed dominantly of subrounded andesitic

TABLE 1: LITHOLOGIC DESCRIPTIONS OF TERTIARY MAP UNITS SHOWN ON FIGURE 2B: NEW ⁴⁰Ar/³⁹Ar DATA PRESENTED IN TABLE 2. GEOLOGIC AND STRATIGRAPHIC POSITIONS OF ⁴⁰Ar/³⁹Ar (NUMBERS) AND GEOCHEMICAL SAMPLES (STARS) PLOTTED ON FIGURE 2A AND 2B, RESPECTIVELY; GPS COORDINATES GIVEN IN DATA REPOSITORY

	Map unit, ⁴⁰ Ar/ ³⁹ Ar Age	Field and Thin Section Characteristics	Interpretation
Age unknown	Tadu—Black Butte andesite dome.	Tan, hornblende-phyric intrusive (?) to extrusive (?) body with glassy groundmass. Pervasive network of randomly oriented fractures, with localized red hydrothermal alteration	In-situ shattering of shallow-level intrusion.
	Tutu—Black Butte lapilli tuff.	White lithic lapilli tuff with local concentrations of blocks; hornblende ± biotite.	Possible silicic block-and-ash-flow tuff.
	Tvdfu—Black Butte volcanic debris flow deposits.	See Tvdf1 for description.	Volcanic debris flow deposit.
	Tap—andesite plug, intrudes unit Tvdf1.	Coarsely hornblende + plag. phyric andesite with microcrystalline matrix.	Shallow-level intrusion of hornblende andesite.
Sequence 6a	Tbat—Red Lake Peak basaltic andesite block and ash flow tuff.*	Dark gray to black andesite, with glassy blocks in a tuff matrix of same composition, unsorted, and massive to very crudely stratified. Very similar in appearance to Taba3, except for higher phenocryst content (Figure 8) and glomerocrysts of clinopyroxene. Thin Section: Phenocrysts: plag. 69.2%, cpx. 9%, Fe-Ti oxide 6%, groundmass 15.5%. Trace amphibole is resorbed / replaced. Groundmass sparse.	Block and ash flow tuff.
	Tvdf2—Volcanic debris flow deposits of Little Round Top	Tvdf2—indistinguishable from Tvdf1 in field characteristics.	Volcanic debris flow deposits.
	Tbl—Basalt lava flows.* 6.80 ± 0.20 Ma (whole rock)	Black glassy, aphyric to crystalline basalt lava flows. Flow 1 is aphyric, with microvesicular, columnar jointed flow interior and a rubbly flow top breccia invaded by flow interior. Flow 2 is olivine- and plagioclase-phyric, with a coarsely vesicular flow top with stretched vesicles. Flow 3 is aphyric with a vesicular horizon or flow top breccia along different parts of its upper contact. Flow 4 is also aphyric; a poorly developed vesicular horizon near the top of this unit may indicate the presence of a very thin (2-m-thick) 5th aphyric lava flow. Thin section: Phenocrysts: iddingsitized olivine >> cpx and plag. Groundmass: plag. > olivine.	Basalt lava flows.
Sequence 6b	Tdd—East Kirkwood dacite or andesite lava dome.	Gray-purple weathering, coherent to brecciated andesite or dacite; appears to locally cross-cut stratigraphy. Coarsely porphyritic plagioclase >> hornblende with holocrystalline groundmass.	Lava dome or thick lava flow.
	Taba3—Sentinels block and ash flow tuff (basaltic andesite*, basaltic trachyandesite*, and trachyandesite*). 6.05 ± 0.12 Ma (plagioclase)	Dark gray to black andesite, with glassy blocks in a tuff matrix of same composition, unsorted, and massive to very crudely stratified. Contrasts with most older andesites at Carson Pass by containing mostly pyroxene (cpx ± opx) instead of hornblende as the mafic phase (Figure 8). Includes prismatically jointed and breadcrust blocks, and matrix-poor vesicular block horizons, and basal slickensides (“skid marks”). Also includes blocky and fluidal andesitic peperite domains several meters across, some with feeder-intrusions but others as detached transported blocks. Thin section: Phenocrysts: 33.4% plag., 6.7% cpx, 6.7% opx, 2.5% Fe-Ti oxide, 50.5% Plag+ cpx glomerocrysts. Groundmass: glass or plagioclase microlites >> Fe-Ti oxide.	Block and ash flow tuff with local “hot block” deposits. Peperite domains formed after deposits became water-saturated within the paleocanyon.
Sequence 5	Tad2—Dark tan andesite lava dome.*	Dark tan andesite, with coherent (nonbrecciated) core that locally cross-cuts stratigraphy (intrusion), passing upward and outward into autobrecciated carapace (lava dome); these pass upward and outward into block-supported monolithic deposits up to a few meters thick, with radially-jointed clasts (hot-block avalanches); these in turn interfinger with debris flow deposits with tan andesite blocks. Large (1-2 cm) hornblende phenocrysts (up to 15%). Thin Section: Phenocrysts: plag. 26.6%, amphibole 11.6%, cpx 3.7%, Fe-Ti oxide 5.6%, lithic fragments 2%. Groundmass (52.5%) holocrystalline plag. >> cpx + Fe-Ti oxide.	Shallow-level intrusion with dome breccia and associated hot-block avalanche deposits.
	Tad1—Purplish white andesite lava dome and tuff.	Purplish white andesite, with coherent (nonbrecciated) core that locally cross-cuts stratigraphy (intrusion), passing upward and outward into autobrecciated carapace (lava dome), in turn passing outward into massive, unsorted tuff breccia (block-and-ash-flow tuff), in turn overlain by an up to 5m thick section of bedded vitric and crystal tuffs. Thin Section: Phenocrysts: plag. 33.1%, amphibole 14.8% (oxyhornblende), Fe-Ti oxide 3.6%. Groundmass (48.5%) holocrystalline plag. >> pyroxene microlites + Fe-Ti oxide. Some glomerocrysts of plag + amphibole.	Shallow-level intrusion with associated dome talus and block-and-ash-flow tuff, overlain by bedded tuff.
	Tvdf1—Kirkwood volcanic debris flow deposits. Age ≥10.49 ± 0.12 Ma (WR date on andesite dike with peperite margins).	Tan ridge-forming, poorly sorted, matrix-supported, massive to crudely stratified cobble/boulder breccias with subrounded to angular clasts, in pebbly sandstone matrix. Dominated by andesite clasts (up to 10 m long), minor mafic clasts and rare granitic basement clasts. Intruded by andesite dikes with peperite margins, and also includes peperite domains with no clear feeder intrusions. Encloses Tad1 and Tad2.	Volcanic debris flow deposits. Interstratified with and intruded by coeval andesite lava domes, block-and-ash-flow tuffs, and <i>in situ</i> and transported peperite domains.

(continued)

TABLE 1: LITHOLOGIC DESCRIPTIONS OF TERTIARY MAP UNITS SHOWN ON FIGURE 2B: NEW ⁴⁰Ar/³⁹Ar DATA PRESENTED IN TABLE 2. GEOLOGIC AND STRATIGRAPHIC POSITIONS OF ⁴⁰Ar/³⁹Ar (NUMBERS) AND GEOCHEMICAL SAMPLES (STARS) PLOTTED ON FIGURE 2A AND 2B, RESPECTIVELY; GPS COORDINATES GIVEN IN DATA REPOSITORY (*continued*)

	Map unit, ⁴⁰ Ar/ ³⁹ Ar Age	Field and Thin Section Characteristics	Interpretation
Sequence 4	Taba2—pink andesite block and ash flow tuff of East Kirkwood.*	Pink-weathering andesite with abundant blocks in tuff matrix of same composition (plag>hbl). Massive (nonstratified) and unsorted. Thin Section: Phenocrysts: plag. 22.9%, amphibole 11.9% (brown amphibole >> green amphibole), Fe-Ti oxides 1.2%, groundmass 64%.) Groundmass: plag. microlites + glass >> Fe-Ti oxide.	Block-and-ash flow tuff.
Sequence 3	Tfu—Upper fluvial deposits (well-sorted, cliff-former).	Similar to Tfl, except it is a cliff former, and is overall slightly better sorted and finer-grained. Accumulation of large log casts found near base of deposit in Little Round Top area are aligned parallel to paleo-transport direction.	Braided stream deposits.
	Trt—Reworked pumice lapilli tuff. Depositional age ≤ 22.9 Ma (multiple single sanidine grains). Tfl—Lower fluvial deposits (poorly sorted, slope-former)	White pumice lapilli tuff, with sanidine and quartz phenocrysts in a vitric ash >> lithic fragment matrix. Thin Section: Rounded pumice lapilli and sanidine phenocrysts > quartz phenocrysts, with lesser lithic fragments of welded tuff. Matrix composed primarily of broken bubble wall shards. Tan to gray slope-forming, stratified, clast-supported cobble conglomerate and lesser pebbly/cobbly sandstone; moderately well-sorted, with subangular to rounded clasts, in medium to thick beds with planar lamination and cut-and-fill structures. Clasts include hornblende and pyroxene andesites.	Miocene fluvial reworking of at least three non-welded Oligocene ignimbrites with inferred source to east of modern-day Sierra Nevada crest. Braided stream deposits.
Probable Sequence 2	Tbai—Round Top basaltic andesite intrusions.* 13.4 ± 1.5 Ma (K/Ar date from Morton et al. 1977.)	Tan to gray cliff-forming coherent intrusion, with hbl>plag ± accessory cpx in microcrystalline groundmass. Hornblende crystals and glomerocrysts up to 1–2 cm, with local clots of hornblende up to 10's of cm in size. Local vesiculated horizons. Well-formed, steeply dipping cooling joints on Round Top and Covered Wagon Peak. Thin Section: Phenocrysts: 15–20% with hornblende > plagioclase = trace cpx and Fe-Ti oxides. Hornblende w/ reaction rims, larger plagioclase phenocrysts resorbed. Holocrystalline groundmass of plag>> Fe-Ti oxide> pyroxene.	Subvolcanic intrusive complex. Reaction rims and resorbed crystals indicate complex magmatic history.
	Tsb—Elephant's Back stratified cobble breccia-conglomerate	Black to gray, moderately well sorted, crudely-stratified, subangular to subrounded, clast-supported pebble- to small cobble breccia/conglomerate. Clasts of andesite >> basalt (aphyric to porphyritic), lesser hypabyssal (holocrystalline) clasts.	Tsb—Streamflow / hyperconcentrated flood flow deposits.
	Tvs—Elephant's Back volcanic lithic sandstones. Intruded by Round Top andesite.	Gray, well sorted, medium-bedded, massive to planar-laminated volcanic lithic sandstones, with thin interbeds of siltstone. Clasts compositions same as map unit Tsb.	Tvs—Stream flow / hyperconcentrated flood flow deposits.
Sequence 2	Tfdf—Interstratified debris flow and fluvial deposits of Castle Point	Gray, ridge forming, poorly sorted matrix-supported, massive to crudely stratified cobble/ boulder breccias with subrounded to angular clasts, interstratified with moderately well-sorted, clast-supported, well-stratified conglomerate and pebbly sandstone, with planar lamination, trough cross-lamination, imbrication, and cut-and-fill structures. Clasts largely andesite, with minor granitic basement clasts, up to 3 m in diameter. One unit exposed in roadcuts along highway 88 is an unusually thick, massive deposit with fine-grained (tuffaceous?) matrix and outsize blocks (up to 10 m) of block-and-ash-flow tuff that resemble map unit Taba1 (described below). Abundant petrified wood fragments also support correlation with map unit Taba1.	Volcanic debris flow deposits and braided stream deposits, possibly triggered by upstream volcanic eruptions. Outsize clasts may represent avalanche blocks.
	Taba1—Carson Pass trachyandesite block and ash flow tuff* and debris flow deposits. 14.69 ± 0.06 Ma (biotite)	Blocks of white, glassy, hornblende + biotite andesite in a tuff matrix of same composition, with charred wood fragments. Massive (nonstratified) and unsorted. Forms discontinuous lenses/bodies that are chaotically interstratified with sandstone/tuffaceous sandstone containing abundant blocks of the white andesite and abundant petrified wood fragments, including a large tree stump. Thin Section of a block from block-and-ash-flow tuff: Phenocrysts: plag. 7.7%, amphibole 15.8%, biotite 1.9%, Fe-Ti oxide 2.5%, groundmass 71.6%. Groundmass: glass>>plagioclase microlites.	Block and ash flow tuffs mixed with debris flow deposits by soft-sediment slumping.
Sequence 1	Ti—Welded and nonwelded ignimbrites.	Sanidine and quartz-bearing rhyolite-welded and lesser nonwelded tuffs, with pumice/ fiamme, and varying percentages and types of crystals and lithic fragments. Locally columnar jointed; may be vitrophyric, devitrified, or vapor phase altered.	Erosional remnants of a complex ignimbrite stratigraphy; correlated with Oligocene calderas in central Nevada (Chris Henry, 2006, personal commun.).

volcanic clasts and minor granitic boulders (Fig. 5D). They include coarse-grained sandstones and pebbly sandstones, and cobble to boulder conglomerate, in thin to thick beds, and are flat laminated to massive, with local cut and fill structures and cross-lamination (Fig. 5E). The common presence of large boulders indicates high axial paleogradients in the paleo-canyon (Fig. 5F). Large, flat-lying log casts are aligned parallel to the trend of the Carson

Pass–Kirkwood paleocanyon at the base of one fluvial unit (Tfl, Fig. 2). Unlike the debris-flow deposits, the cobble- to boulder-sized clasts in the fluvial deposit are not monolithic; however, the restricted range in clast types and general angularity of clasts suggest that andesite source areas were not far away. Map units composed entirely of streamflow deposits, with no interbeds of debris-flow deposits, form the most resistant outcrops of the central Sierra Nevada

(Fig. 5G), other than the hypabyssal intrusions. In contrast, map units consisting of interstratified streamflow and debris-flow deposits are less resistant.

Lava Flows

Except for volumetrically minor lava-dome breccias associated with andesite intrusions and block and ash flow tuffs, there are no andesite lava flows in the study area. Basalt

West

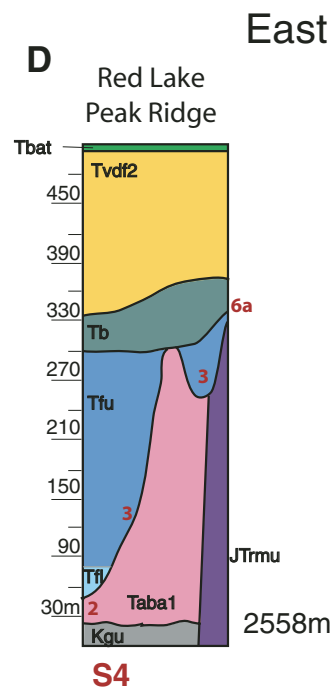
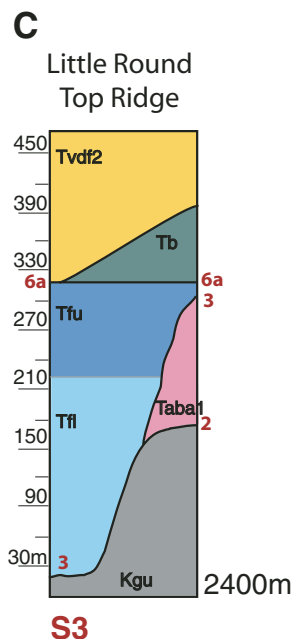
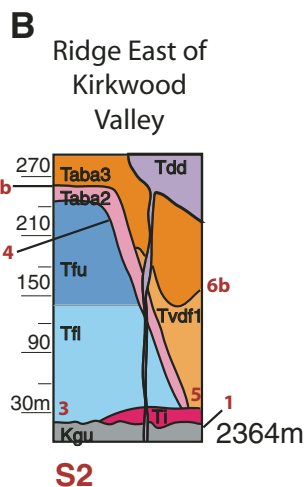
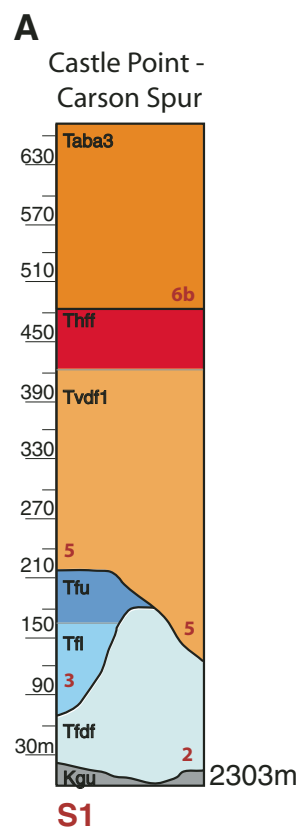


Figure 3. Composite lithostratigraphic columns showing unconformities (1–6a, 6b in red, also shown in Fig. 2A), and thicknesses of the map units at locations S1–S4 (plotted in Fig. 2B). The stratigraphy is divided into six unconformity-bounded sequences, each sequence numbered to correspond to the unconformity that underlies it. Elevations at the base of each section are given on lower right side of each column. Inset table summarizes the geometric parameters of each unconformity.

Unconformity Number	Relief (m) minimum, maximum	Maximum Gradient	Mappable Lateral Extent (Km)
6a	36, 303	.48	6.0
6b	121, 303	.06	5.0
5	85, 200	.32	4.2
4	167, 227	.32	1.4
3	133, 315	.06	3
2	170, 291	.23	1.5
1	12, 650	.50 in granite .70 in metamorphic	8

lava flows are restricted to a single section of five flows at Carson Pass between Red Lake Peak and Little Round Top; small olivine basalt intrusions are along the crest and east of it (Hagan and Busby, 2007).

Peperites

Peperites occur within paleocanyon fill of the Mehrten Formation at many localities close to the crest of the Sierra Nevada (Busby et al., 2007), but they were closely examined in the Kirkwood area, where they are very well exposed in large outcrops (Figs. 5H, 5I, and 6). These formed by interaction of magma and wet sediment, and include both *in situ* peperites and resedimented peperites, inferred to have been transported from vent areas by slides or debris flows.

One stage of peperite generation at Kirkwood has been dated as 10.49 ± 0.12 Ma (Table 2), the age of a peperite-margined dike on the north side of Kirkwood Valley (Figs. 2, 5H, and 5I). This dike intrudes debris-flow deposits (Tvd1) of sequence 5. Another stage of peperite generation at Kirkwood was dated by peperite domains with clear feeder intrusions within the 6.05 ± 0.12 Ma (Table 2) Sentinels block and ash flow tuff (Taba3); the best examples of these peperites occur at the Sentinels and Martin Point, close to the Thunder Mountain trail (Fig. 2). The features displayed there are interpreted to represent both *in situ* and transported peperite (Fig. 6), and record processes summarized in Figure 7.

Juvenile peperite components are ash- to block-sized (to several meters across) andes-

itic and/or trachyandesitic vitric clasts with 20%–40% plagioclase, 5%–15% pyroxene, and <5% hornblende. These clasts are of variable vesicularity (5%–20%) but are typically unvesiculated or poorly vesiculated (<5%). The juvenile clasts are both blocky (brittle) and fluidal (ductile) (in the sense of Busby-Spera and White, 1987); many domains comprise a mixture of both morphologies. Elongate fluidal clasts may display a crude alignment. Analysis of host sediment suggests that it was derived from several sources, including: (1) heterolithic subrounded hornblende-phyric andesitic sand and gravel identical to that in the Tvd1 debris-flow deposits, (2) massive, blocky to splintery, poorly vesicular (<15%) pyroxene-phyric vitric ash lapilli identical to that of the matrix

Figure 4. Cross sections and interpreted photomosaics, Carson Pass–Kirkwood Valley area. Lines of sections and key to map units and unconformities are shown in Figure 2. (A) Longitudinal cross section along the axis of the Carson Pass–Kirkwood paleocanyon (A–A'). The floor of the paleocanyon drops to the southwest, consistent with paleocurrent data (Fig. 2). No cross section displays all the unconformity-bounded sequences, due to lateral shifting of the erosional thalweg with time (see B–E). Unconformity 3 is a very steep buttress unconformity at the eastern (right) side of the cross section, where fluvial deposits overlie metamorphic rocks, and a much gentler unconformity where the fluvial deposits overlie Mesozoic granitic rocks in the central part of the cross section. Unconformity 5 cuts through all older sequences to granitic basement at the western side of the cross section, and unconformity 6b downcuts precipitously through sequence 5, nearly to bedrock, at the westernmost end of the section. (B) Interpreted photomosaic illustrating unconformities 1, 3, and 6a along the Sierran crest, viewed north toward Red Lake Peak (Fig. 2). Relations shown here are summarized schematically in Figure 3D. The granitic basement rises rapidly (up-paleocanyon) between Little Round Top Ridge and Red Lake (A; see sections 3 and 4, Fig. 3); therefore, only the upper fluvial unit (Tfu) is present in this area. On the left (west) side of the photo, bedding in the upper fluvial unit (Tfu) clearly onlaps unconformity 3, a very steep erosional unconformity cut into the 14.69 ± 0.06 Ma Carson Pass trachyandesite block and ash flow tuff of sequence 2 (Taba1); the same unconformity drops to the right (east), just out of direct view (arrow pointing to unconformity 3). A less dramatic but clear buttress unconformity is also visible between the upper fluvial unit (Tfu) and the metamorphic basement rocks (JTrmu) on the far right (easternmost) side of the photo (labeled 3). The sequence 2 Carson Pass trachyandesite block and ash flow tuff (Taba) also is in buttress unconformity against basement metamorphic rocks (JTrmu), along a contact that dips $\sim 70^\circ$ toward the viewer (Fig. 2), but in this view the contact is hidden in a gully behind a ridge (arrow pointing to unconformity 1). Unconformity 6a is a gently sloping surface that represents a 4–8 m.y. time gap where the 6.80 ± 0.20 Ma basalt lava flows (Tb1) overlie the upper fluvial unit (Tfu), and an 8 m.y. time gap where the basalt lava flows overlie the trachyandesite block and ash flow tuff (Taba1). The basalt lava flows pinch out eastward (up-paleocanyon) against unconformity 6a (Fig. 4A). The basalt unit is conformably overlain in apparent conformity by the volcanic debris-flow deposits of Little Round Top (Tvd2). This in turn is overlain in apparent conform by the sequence 6a basaltic andesite block and ash flow tuff of Red Lake Peak (Tbat), which forms the topographically highest unit in the Carson Pass–Kirkwood paleocanyon. (C) Transverse cross section across the part of the Carson Pass–Kirkwood paleovalley, along the ridge east of the Kirkwood Valley (C–C', Fig. 2). Relations shown here are summarized schematically in Figure 3B. Repeated reincision has produced closely spaced erosional unconformities (3–6); unconformities are steepest on transverse cross sections, marking the shifting of the paleocanyon thalweg with time (unconformities 4–6a). (D) Interpreted photomosaic illustrating outcrop expression of unconformity surfaces, and lithofacies relationships to these surfaces, in the area boxed in C. View is toward the northeast, as seen from ski lift chairs on the ridge west of Kirkwood Valley. Although the contact between the lower and upper fluvial units (Tfl and Tfu) is somewhat irregular on the outcrop scale, it appears conformable on the map scale (Fig. 2), so that contact is not numbered as an unconformity; these units dip gently toward the west. The sequence 3 fluvial units were deeply eroded to produce unconformity 4, which is overlain by pale pink andesite block and ash flow tuff (Taba2); this tuff presumably had an originally flat upper surface, which in turn was incised to form unconformity 6b. The sequence 6a andesite block and ash flow tuff of the Sentinels (Taba3) shows soft sediment deformation of crude bedding (red squiggly lines) where it slumped into the paleochannel represented by unconformity 6b. The east Kirkwood dacite dome (Tdd) intrudes sequences 4, 5, and 6b (Fig. 3B), forming the white rock visible in the top center of the photograph. (E) Transverse cross section across the part of the Carson Pass–Kirkwood paleovalley, along the ridge west of the Kirkwood Valley (B–B'–B'', Fig. 2). Some of the relations shown here are summarized schematically in Figure 3A. Strata of sequence 2, the interstratified debris-flow deposits and fluvial deposits of Castle Point (Tfd, Fig. 2), are here unconformably overlain by sequence 5 volcanic debris-flow deposits of Kirkwood (Tvd1), representing a time gap of ~ 8 m.y.; the lower and upper fluvial units (Tfl and Tfu) intervene just out of the line of section (Fig. 2). The slickensides at the base of the andesite block and ash flow tuff of the Sentinels (Taba3) (described in text) occur where it overlies granitic basement at Melissa Corey Peak. The unconformity beneath this unit (6b) is unusually flat for a transverse line of section, but it cuts very rapidly downsection immediately west of this line of section (as shown in the westernmost end of A). The steep contact between the basaltic andesite intrusion of Round Top (Tbai) and sequence 5 is interpreted as erosional rather than intrusive, because the Round Top intrusion has an older date (see text).

of the Taba3 block and ash flow deposits, and (3) buff-colored, unvesiculated, well-sorted, blocky vitric-rich ash-lapilli tuff or sandstone, interpreted as a lacustrine or pond suspension deposit (Fig. 6D). The host sediment is typically massive, but in the suspension deposit is locally parallel laminated. Ductile peperite domains at Kirkwood are generally smaller in cross section (<1 – 50 m across) than the brittle domains (<1 – 300 m across). Some of the ductile domains are also clearly associated with feeder intrusions, which are commonly dike like, but many domains have no clear feeder intrusions. Where feeder intrusions are visible, juvenile clast dispersal of at least 200 m can

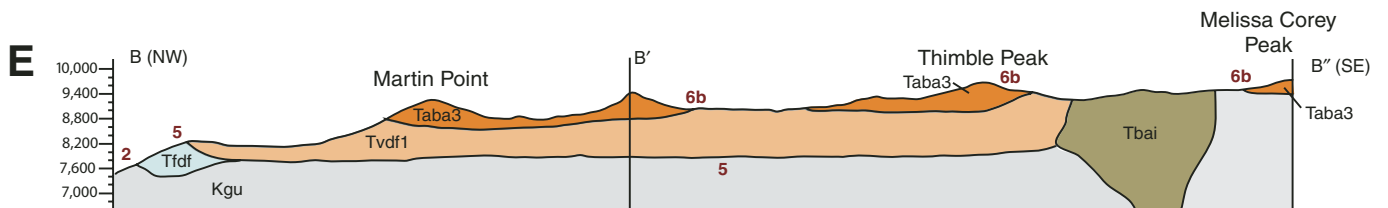
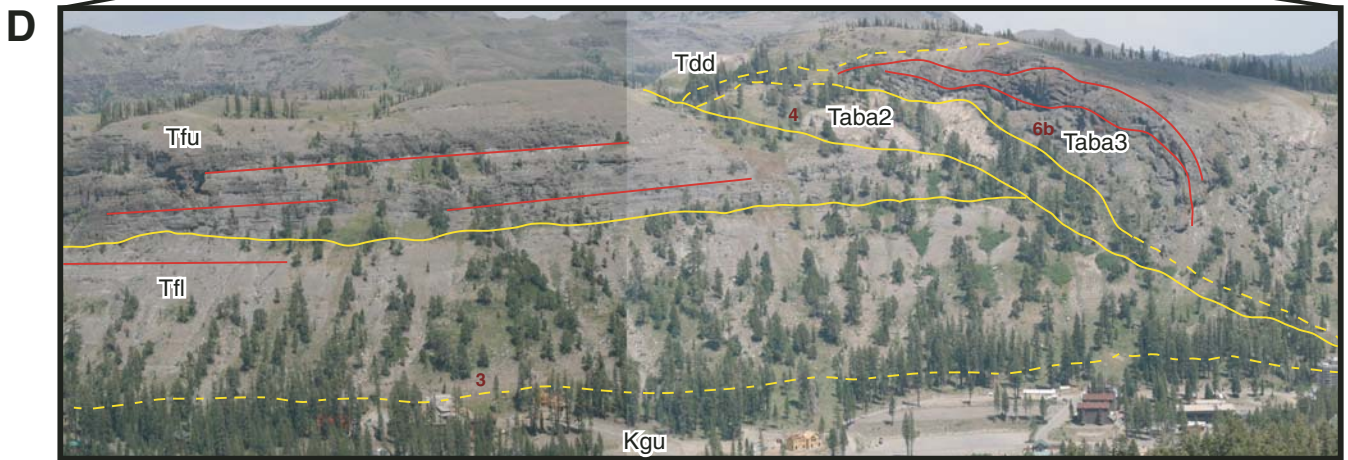
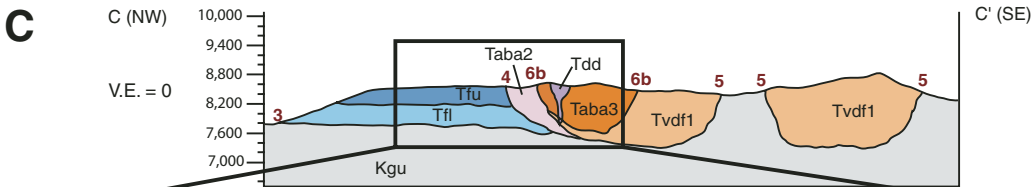
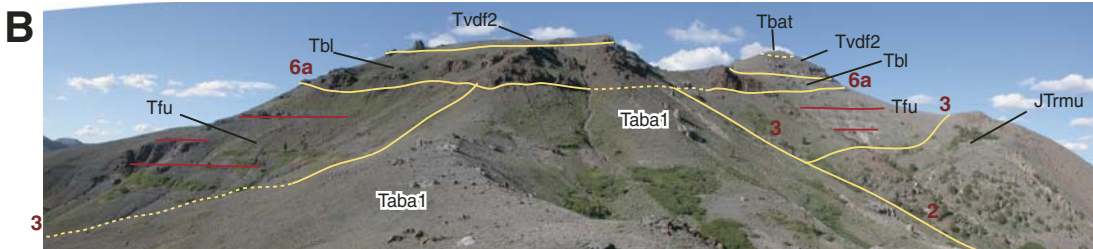
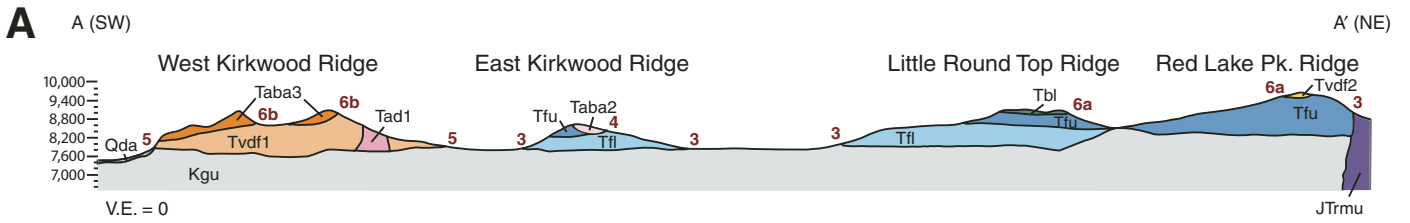
be recognized. Peperite domains are also commonly associated with distinctive haloes of reddish hydrothermal alteration.

Many of the peperite domains are not *in situ* and were either ripped up and transported within overriding debris-flow and block and ash flow deposits, or underwent downslope sliding during or shortly after they were generated, or both. For example, the peperite-bearing Sentinels block and ash flow tuffs (Taba3) also display large (to tens of meters) rotated and variably deformed domains of the underlying heterolithic debris-flow deposits (Tvd1, Fig. 6E) and buff-colored parallel-laminated vitric ash-lapilli tuff. Many peperite domains

and their host deposits in the Kirkwood area also display internal and/or basal slickensided steep ($>50^\circ$) slide planes (Fig. 6A). The absence of feeder intrusions to the majority of the peperite domains also supports the interpretation of movement of the peperite domains from the site of their initial formation.

SEQUENCE STRATIGRAPHY

This section provides a description of each unconformity surface, followed by a condensed description and interpretation of the map units within each sequence (shown in Fig. 2 key; for more complete lithologic descriptions and



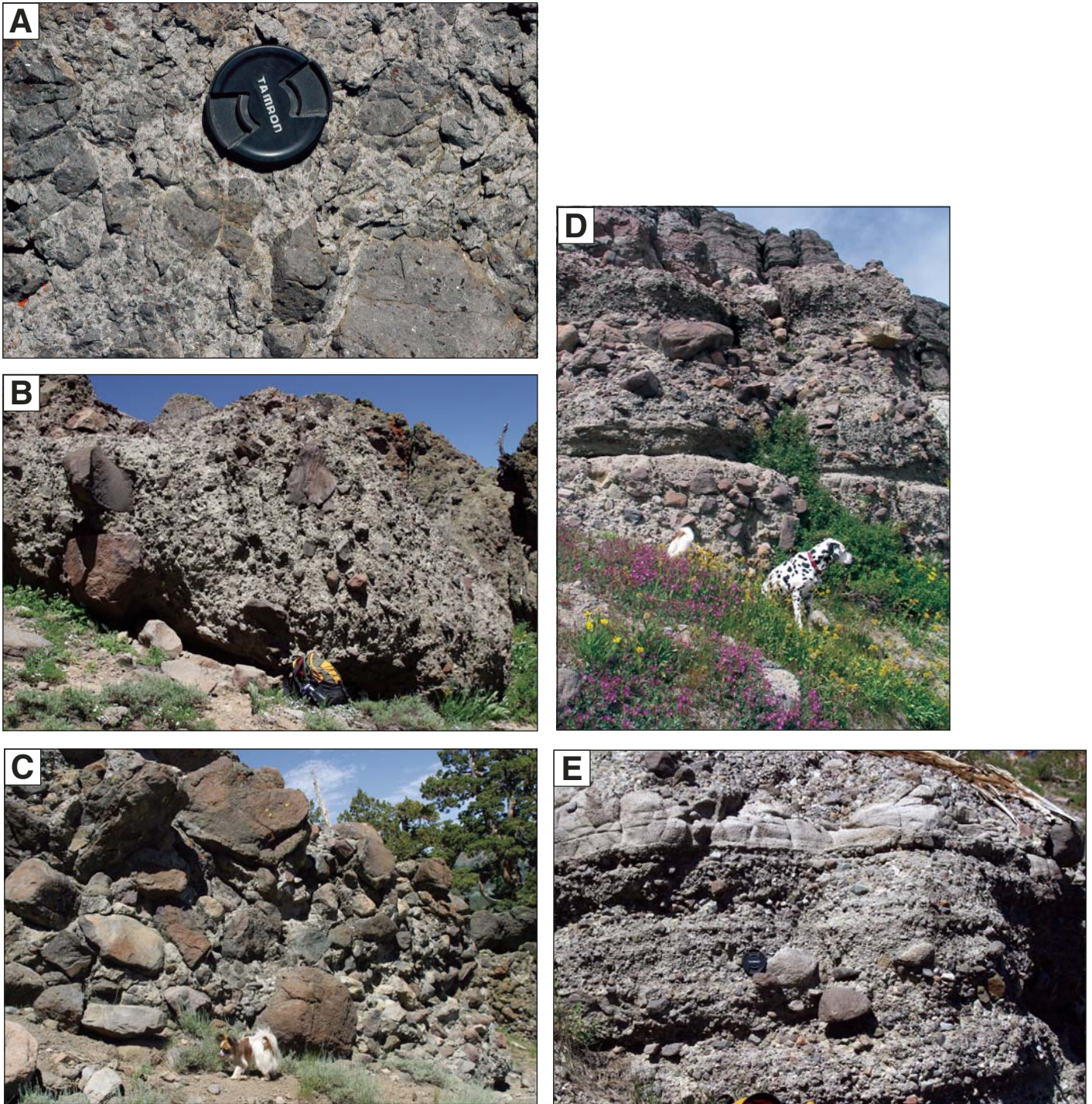


Figure 5. Representative lithofacies photos. (A) Andesite block and ash flow deposit: medium gray angular *in situ* and prismaticly jointed poorly vesiculated blocks of hornblende-phyric andesite in paler gray, coarse ash- to coarse lapilli-sized matrix of clasts of same composition (Tab3 facies, Martin Point, Kirkwood, Fig. 2). (B) Massive, unsorted, coarse-grained volcanic debris-flow deposit with random clast orientation. All of the debris-flow deposits have a variety of andesite clast types, mostly angular, in a volcanic lithic sandstone matrix. (C) Stratified, inverse to normally graded volcanic debris-flow deposits (overlain by well-stratified streamflow deposits at top of photo in background). (D) Boulder conglomerate, clast-supported with subangular to rounded clasts, interpreted as streamflow deposits. (E) Stratified pebble to cobble conglomerate and massive to planar-laminated granule sandstone, interpreted as hyperconcentrated flood-flow or steamflow deposits. (Continued on following page.)

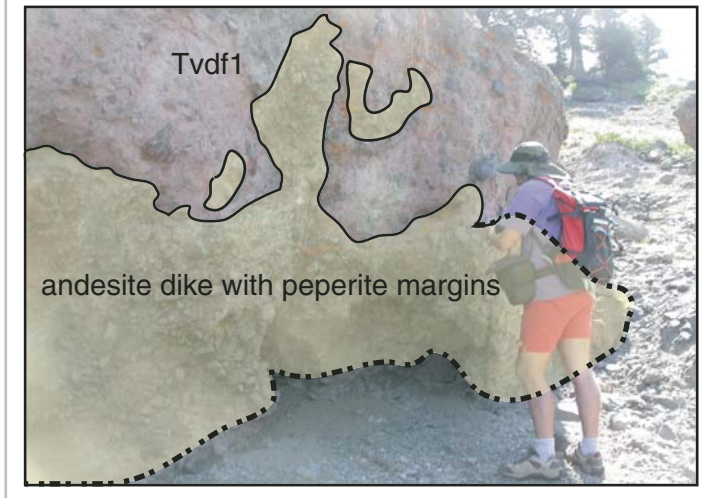
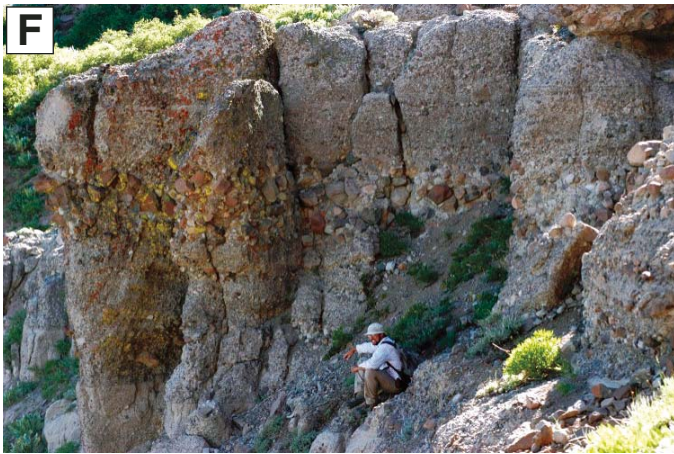


Figure 5 (continued). (F) Sequence of volcaniclastic (andesitic) parallel to cross-bedded pebbly sandstones with interbedded matrix-supported massive cobble-boulder bed. Interpreted as hyperconcentrated flood-flow and/or streamflow deposits with debris-flow deposits interbed. (G) Outcrop appearance of thick, cliff-forming andesite-clast fluvial deposits (Tfu, Fig. 2). The white outcrop is the reworked pumice lapilli tuff (Trt), which fills a deep and narrow channel cut into the slope-forming lower fluvial unit (Tfl, Fig. 2). Excised thickness of white tuff in photo is 20 m. (H) Outcrop photo and line drawing interpretation of the 10.50 ± 0.12 Ma andesite dike, which forms peperite within the volcanic debris-flow deposits of Kirkwood (Tvd1, Fig. 2). (I) Closeup of jigsaw textures and dispersed fragments around the margins of the peperite dike.

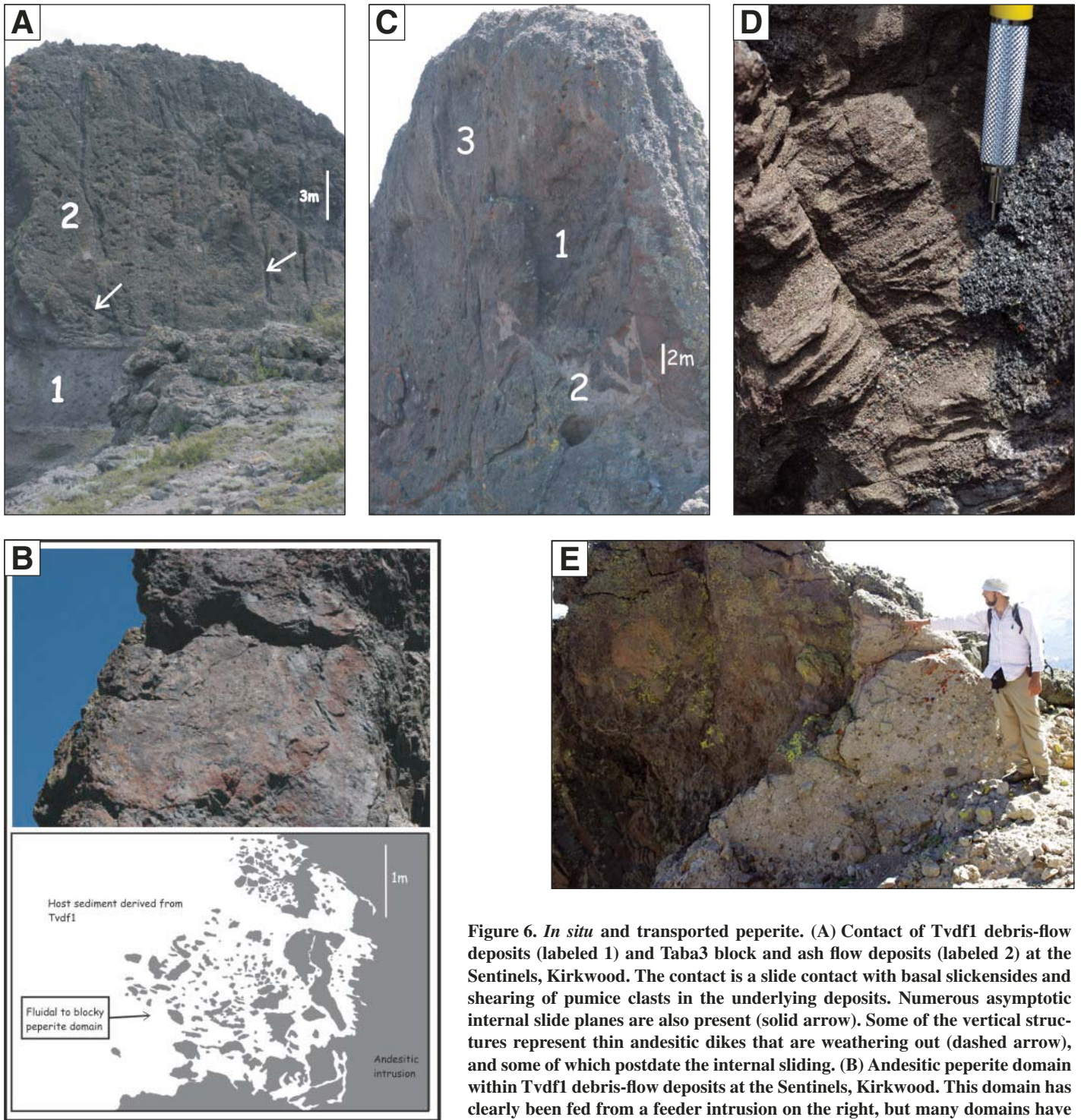


Figure 6. *In situ* and transported peperite. (A) Contact of Tvdf1 debris-flow deposits (labeled 1) and Taba3 block and ash flow deposits (labeled 2) at the Sentinels, Kirkwood. The contact is a slide contact with basal slickensides and shearing of pumice clasts in the underlying deposits. Numerous asymptotic internal slide planes are also present (solid arrow). Some of the vertical structures represent thin andesitic dikes that are weathering out (dashed arrow), and some of which postdate the internal sliding. (B) Andesitic peperite domain within Tvdf1 debris-flow deposits at the Sentinels, Kirkwood. This domain has clearly been fed from a feeder intrusion on the right, but many domains have been detached from the feeders during incorporation and transport within

both Tvdf1 and Taba3 deposits. The host sediment here also includes a distinctive buff colored parallel-laminated fine-grained vitric sandstone that is interpreted as a subaqueous suspension deposit. (C) Peperite domain comprising large coherent mass of andesite (1) and large detached blocks in a host sediment (2) that resembles the Tvdf1 matrix. The domain has been ripped up, detached and transported (?) within a Taba3 block and ash flow deposit (3). (D) The andesitic peperite at the Sentinels was generated when magma mingled with several types of wet sediment, including debris-flow deposits (Tvdf1), wet block and ash flow deposits (Taba3), and, as illustrated here, a distinctive buff-colored vitric-rich parallel-laminated and normally graded sandstone with componentry identical to hydrothermally altered Taba3 clasts. The parallel lamination is commonly disrupted or destroyed during mingling with the magma, but is locally preserved. The tip of the pencil is on a juvenile andesitic clast. This deposit is interpreted as a suspension deposit formed in a (E) transported peperite consisting of a large clast of peperite within a debris-flow deposit.

TABLE 2. SUMMARY OF ⁴⁰AR/³⁹AR DATA FOR CARSON PASS–KIRKWOOD AREA

Sample name, map unit, and sample number	Rock description	Mineral dated	Age (Ma)
Trachyandesite block and ash flow tuff of Carson Pass (Taba1), CP-30	Blocks of white, glassy, hornblende + biotite in vitric ash + crystal matrix, with rare charred wood fragments; matrix of same composition.	Biotite	14.69 ± 0.06
Reworked pumice lapilli tuff (Trt), CP-29	Massive, white, nonwelded pumice lapilli tuff, consisting of rounded pumice lapilli in a matrix of sanidine and quartz phenocrysts, bubble wall shards, and minor welded tuff fragments.	Plagioclase Single sanidine ages	14.1 ± 0.7 22.9 ± 0.1 23.2 ± 0.1 23.2 ± 0.1 23.4 ± 0.1
Peperite dike in volcanic debris-flow deposits of Kirkwood, CP-20	Andesite dike with peperite margins, cross cuts the volcanic debris flow of Kirkwood (Tvd1).	Fusions of several grains Plagioclase	10.49 ± 0.12
Basalt lava flows of Carson Pass (Tbl), CP-62	Black, glassy, dominantly aphyric lava flows, with flow-tops marked by flow breccias or vesicular horizons.	Whole rock	6.80 ± 0.20
Andesite block and ash flow tuff of the Sentinels (Taba3), CP-61	Black, glassy blocks of hornblende + clinopyroxene + plagioclase andesite in vitric ash + crystal matrix; matrix of same composition.	Plagioclase	6.05 ± 0.12

Note: All errors 2σ. For samples with two ages reported, the age with the smaller error is the one used in the text. Locations of samples are plotted on Figure 2 by age, and global positioning system coordinates of sample localities are given in the GSA Data Repository (see text footnote 1).

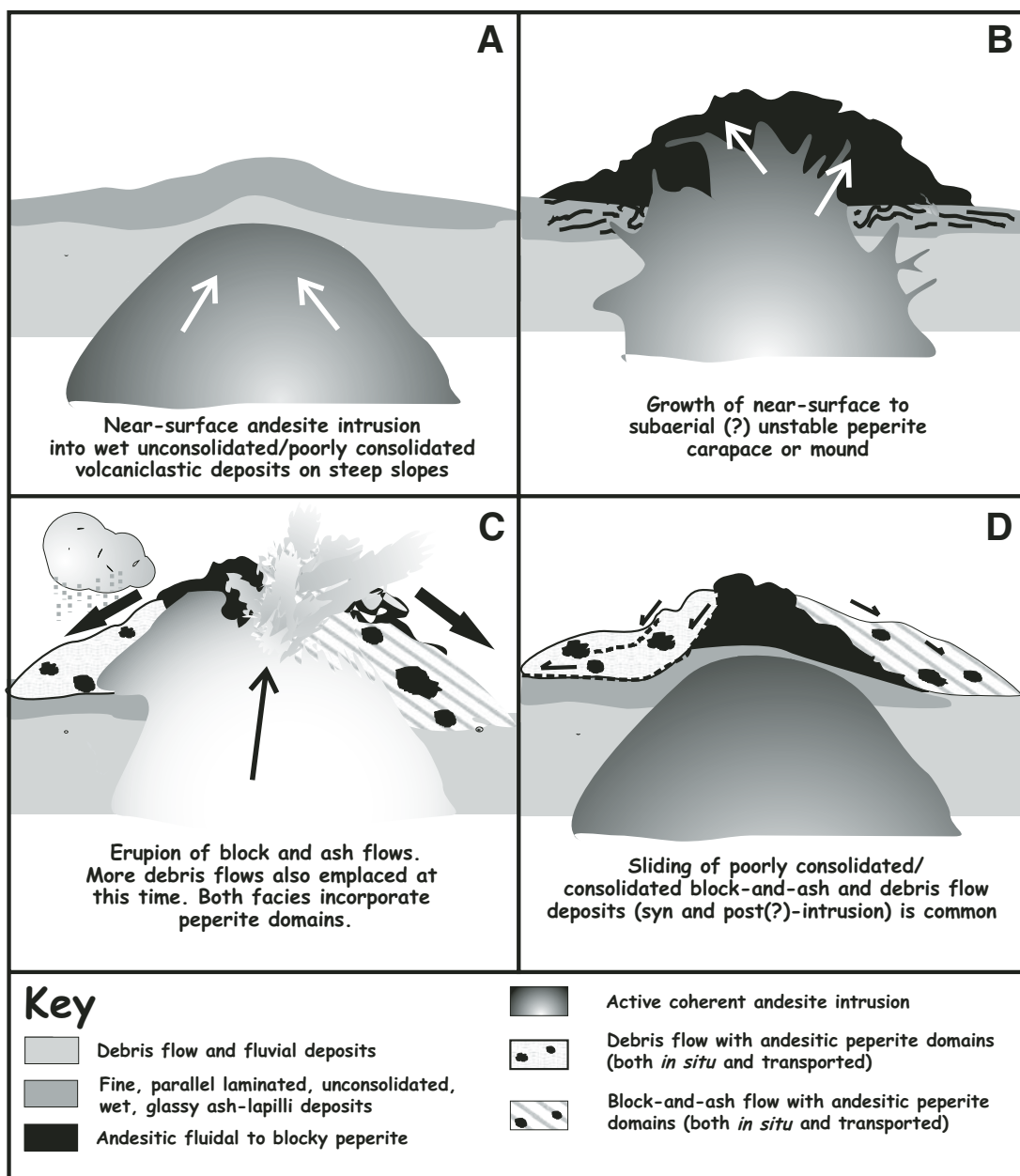


Figure 7. Interpretive diagram of *in situ* and transported peperite.

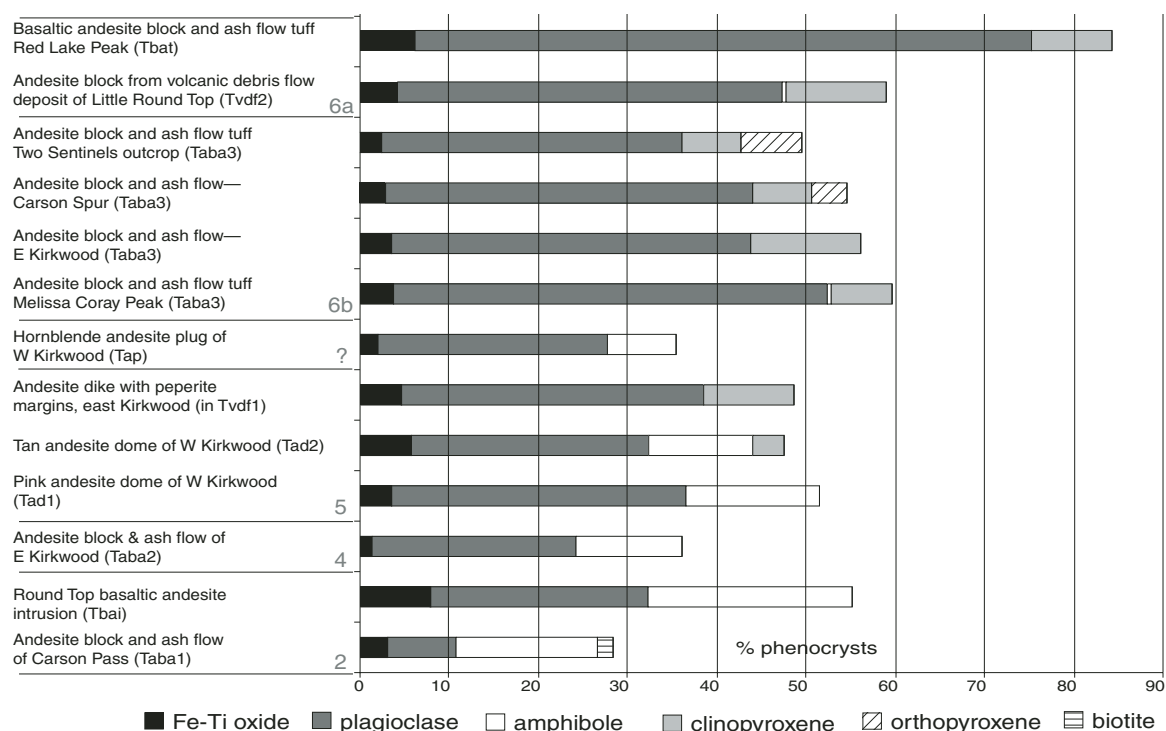


Figure 8. Modal analyses of intrusive and proximal extrusive Miocene rocks (sequences 2, 4, 5 and 6, Figure 2A and Table 1; sequence numbers shown in red). One thin section per analysis, with 1000 counts per thin section. Global positioning system positions of samples are given in GSA Data Repository (see footnote 1). The mafic phase is dominantly hornblende in sequences 2–5, and dominantly pyroxene in the youngest sequence (6). Biotite is only found in the oldest Miocene unit (Taba1 of sequence 2).

interpretations, see GSA Data Repository¹). Composite stratigraphic columns (Fig. 3) depict maximum unit thickness, maximum relief on unconformity surfaces, and schematic representations of contact relationships. Geologic cross sections and annotated photomosaics illustrate the geometries of unconformities and the distributions of sequences (Fig. 4). Thin-section characteristics are described in Table 1, and modal analyses are presented in Figure 8. The ages of dated map units are referred to here, with geochronological data presented in the following section (Fig. 9; Table 2).

Sequence 1

Unconformity 1 (Figs. 2 and 3) can be mapped as either the contact between granitic basement and erosional remnants of Oligocene ignimbrites (Ti, Fig. 2), or as the walls and floor of the entire paleocanyon. The basement-ignimbrite contact in the Carson Pass–Kirkwood paleocanyon is preserved in a small area along the east

side of the Kirkwood Valley, for a distance of only 1 km in a direction roughly subparallel to the paleocanyon axis (estimated vertical relief of 36 m and maximum gradient of 3°). In Figure 3, however, we describe unconformity 1 as the walls and floor of the entire paleocanyon, with a lateral extent of ~8 km, vertical relief of as much as 650 m, and with maximum gradient of 50° on granitic basement and 70° on metamorphic basement. We do this for the following reasons. (1) Basement clasts are very rare within this or other central Sierran paleocanyon fills, suggesting to us that there was no appreciable widening or deepening of this or other paleocanyons during deposition of Tertiary strata. (2) All of the younger unconformities (unconformities 2–6) record reincision into Tertiary paleocanyon fill, but not into bedrock below that. Therefore, unconformity 1 merges with all of the younger unconformities at the paleocanyon walls or floor. (3) Some stretches of other central Sierran paleocanyons preserve sequences as thick as 200 m of as many as 6 petrographically distinct ignimbrites (Fig. 10A; Slemmons, 1953, 1966). Slemmons (1966) inferred that the ignimbrite once formed a relatively continuous sheet. (4) In other central Sierran paleocanyons, we have observed erosional remnants of welded

ignimbrite high on paleolegges created by joints in the granitic basement (Fig. 10B; Busby et al., 2007). All of these data suggest that the main canyon-carving event in the central Sierra Nevada (referred to as unconformity 1 in the Carson Pass–Kirkwood paleocanyon) occurred before the ignimbrites were deposited, and that the ignimbrite fills of the paleocanyons were originally very thick, but were largely removed by a major reincision event in the early Miocene (Fig. 10B).

Welded and Nonwelded Ignimbrite (Ti)

Ignimbrites in the Carson Pass–Kirkwood paleocanyon are poorly exposed and laterally restricted, but include both welded and nonwelded deposits, possibly of more than one mineralogical variety (Table 1). Sierran ignimbrites are considered a distal facies likely erupted from Oligocene calderas in Nevada (Henry et al., 2003; Hinz et al., 2003; Faulds et al., 2005a).

Sequence 2

Unconformity 2 occurs at the western and eastern ends of the map area (Fig. 2). In the west, it forms a channel cut into granitic basement (Figs. 3A and 4E) and filled with interstratified

¹GSA Data Repository item 2007135, 7 sample locations, geochemical data, and ⁴⁰Ar/³⁹Ar age data, is available at <http://www.geosociety.org/pubs/ft2007.htm> or by request to editing@geosociety.org.

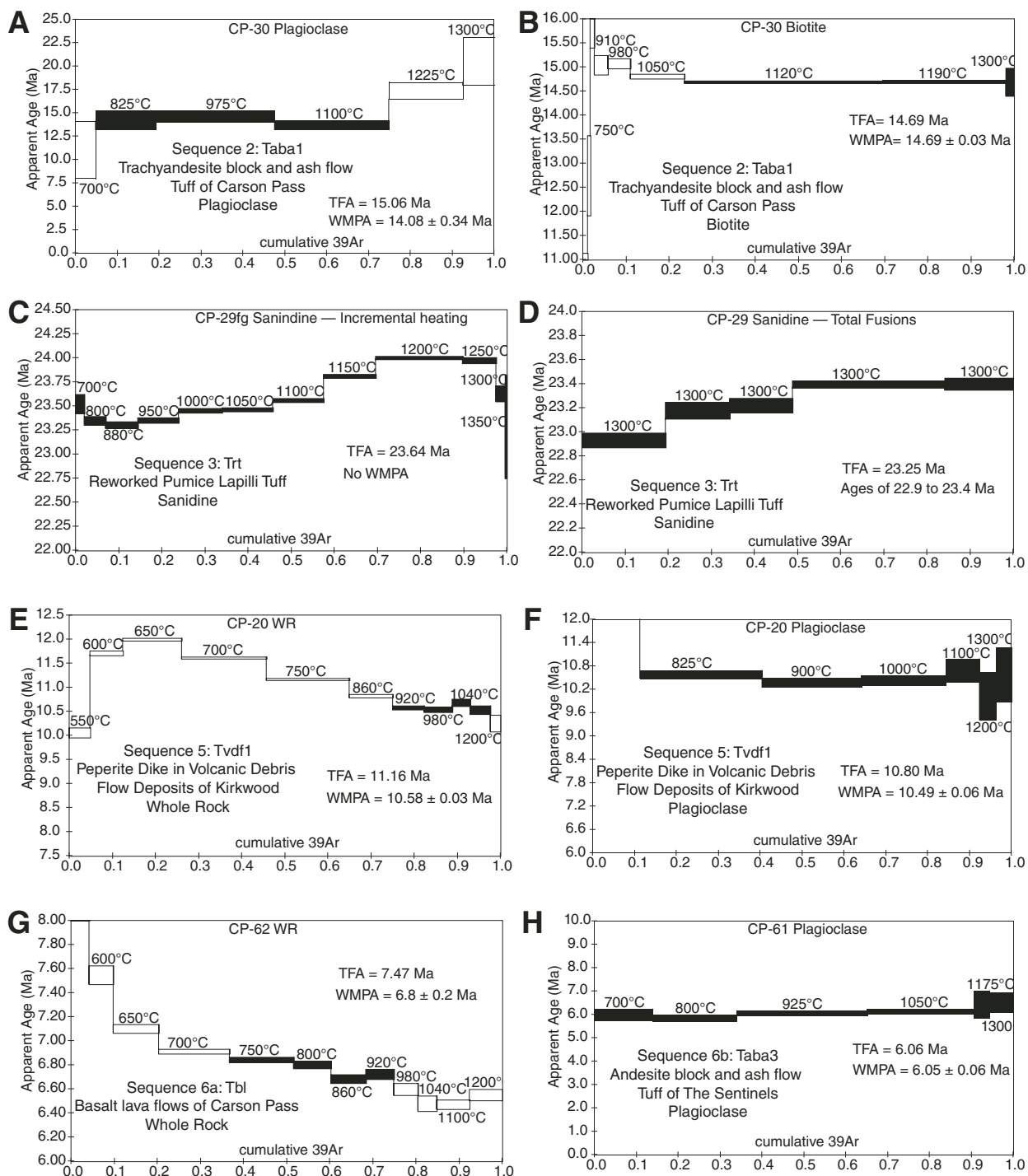
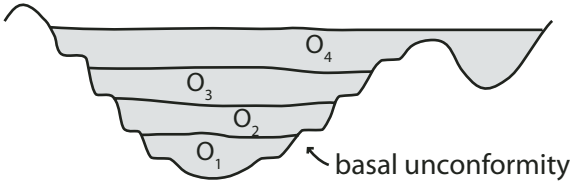
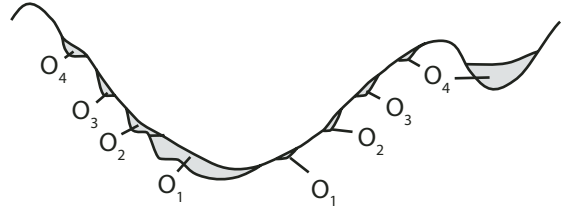


Figure 9. The $^{40}\text{Ar}/^{39}\text{Ar}$ Age spectra for dated sample from the Carson Pass–Kirkwood area. See Figure 2 and Table 1 for sample localities and descriptions of units. Global positioning system coordinates for samples, tabulated argon data, inverse isochron plots, K/Ca spectra, and additional technical details regarding the analyses are included in the GSA Data Repository (see footnote 1). (A) Plagioclase age spectrum for the Carson Pass trachyandesite block and ash flow tuff (Taba1), sequence 2. (B) Biotite age spectrum for the Carson Pass trachyandesite block and ash flow tuff (Taba1), sequence 2. (C) Age spectrum from incremental heating experiment for a bulk sanidine separate from the same unit as D. (D) Total fusion analyses (plotted as age spectrum by increasing age) of sanidine from a reworked pumice lapilli tuff (Trt), sequence 3, suggesting at least three late Oligocene–early Miocene sources for this deposit, which fills a channel cut into the middle Miocene, lower fluvial deposits (Tff), sequence 3. (E) Whole-rock age spectrum for andesite dike with peperite margins in the Kirkwood volcanic debris flow (Tvd1), sequence 5. (F) Plagioclase age spectrum for andesite dike with peperite margins in the Kirkwood volcanic debris flow (Tvd1), sequence 5. (G) Whole-rock age spectrum for the basalt lava flow of Carson Pass (Tbl). WMPA—weighted mean plateau ages; TFA—total fusion age. (H) Plagioclase age spectrum for andesite block and ash flow tuff of the Sentinels, sequence 6b.

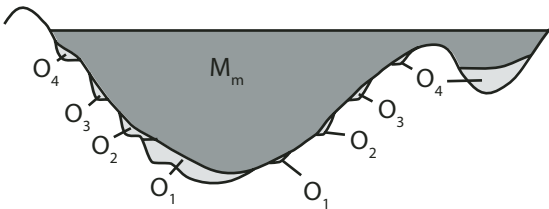
A Oligocene ignimbrites erupted in central Nevada fill paleocanyon incised into Mesozoic basement rocks.



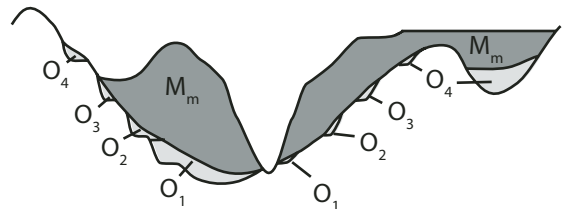
B Re-incision 1: Early Miocene (ca 18–15 Ma) erosion of Oligocene ignimbrites.



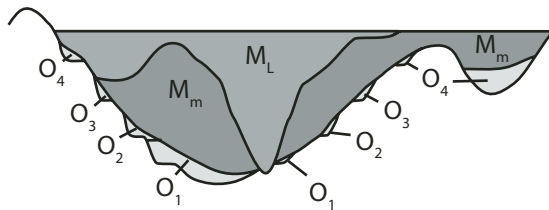
C Middle Miocene andesitic volcanic-volcaniclastic rocks fill paleocanyon.



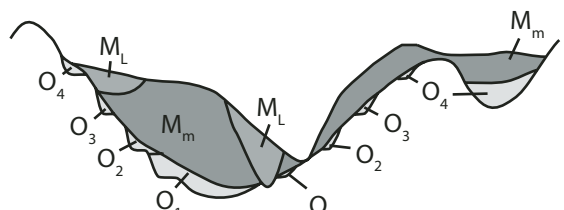
D Reincision 2: Middle Miocene (ca 10 Ma) erosion, locally to bedrock.



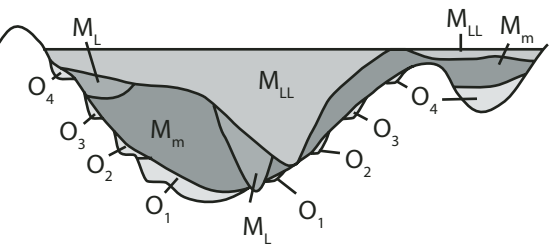
E Late Miocene andesitic volcanic-volcaniclastic rocks fill paleocanyon.



F Reincision 3: Late Miocene (ca 7 Ma) erosion, locally to bedrock.



G Late-late Miocene andesitic volcanic-volcaniclastic rocks fill paleocanyon.



H Present Day

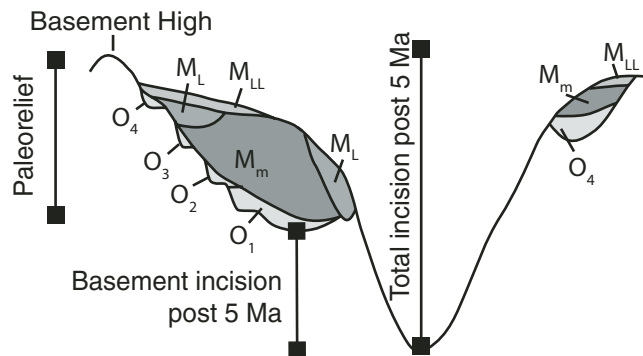


Figure 10. Model for the topographic evolution of the central Sierra Nevada, modified from Wakabayashi and Sawyer (2001) in order to highlight the important re-incision events inferred here for the central Sierra Nevada. Reincision events are inferred from the deep and steep-sided unconformities shown in Figure 2B: reincision event 1 corresponds to unconformity 2, reincision event 2 corresponds to unconformity 5, and reincision event 3 corresponds to unconformity 6.

volcanic debris-flow and fluvial deposits of Castle Point (Tfdf). In the east, unconformity 2 forms a paleocanyon with its preserved wall cut steeply into Jurassic metamorphic rock (Fig. 4B) and less steeply into Cretaceous granite (Fig. 3C); this canyon is filled by white- to buff-colored trachyandesite block and ash flow tuffs of Carson Pass (Taba1). Unconformity 2 has a maximum vertical relief of 291 m, a maximum gradient of 23°, and a lateral extent of 1.5 km (Fig. 3). This deep unconformity is referred to as reincision 1 in Figure 10B.

Trachyandesite Block and Ash Flow Tuff and Debris-Flow Deposits of Carson Pass (Taba1)

Trachyandesite block and ash flow tuffs north of Carson Pass (Fig. 2) are the oldest Miocene primary volcanic strata in the area. This is the only Miocene unit bearing biotite (Fig. 8), which gives an $^{40}\text{Ar}/^{39}\text{Ar}$ date of 14.69 ± 0.06 Ma (Table 1; Fig. 9B). These light colored block and ash flow tuffs are complexly interstratified with deposits containing a more heterolithic pebbly sandstone matrix. We infer that as block and ash flows traveled down the paleocanyon, some of them mixed with water and accidental volcanic detritus to form volcanic debris flows. The block and ash flow tuffs in this unit contain carbonized wood, a feature common in block and ash flow tuffs (e.g., Mount Merapi; Camus et al., 2000). The interstratified debris-flow deposits contain abundant petrified wood. This supports the interpretation that the debris-flow deposits mixed with water and cooled during transportation, whereas the block and ash flow tuff was deposited hot and therefore able to char wood fragments.

Interstratified Volcanic Debris-Flow and Fluvial Deposits of Castle Point (Tfdf)

This map unit is composed of approximately subequal amounts of interstratified coarse-grained fluvial and debris-flow deposits (Table 1). The debris-flow deposits locally contain blocks of light colored block and ash flow tuff as large as 10 m, similar to the block and ash flow tuff of Carson Pass in color and mineralogy (Taba1). Like the debris-flow deposits interstratified with the block and ash flow tuff of Carson Pass (Taba1), the debris-flow deposits at Castle Point (Tfdf) contain abundant petrified wood fragments. Both map units overlie granitic basement and are overlain in erosional unconformity by sequence 3. Fluvial sandstones interstratified with debris-flow deposits of Castle Point (Tfdf) show well-developed medium-scale trough cross bedding that suggests an east-to-west transport direction (Fig. 2). For all of these reasons, we interpret the Castle Point map unit (Tfdf) to be the down-paleocanyon, more

vent distal equivalent of the Carson Pass map unit (Taba1), and we infer that they are approximately the same age (Fig. 2B).

Volcanic Lithic Sandstone and Stratified Cobble Conglomerate Breccia of Elephant's Back (Tvs and Tsb)

A section of volcanic lithic sandstones, overlain by volcanic breccia conglomerate, forms Elephant's Back, a prominent peak along the range crest south of Carson Pass. This section is isolated from the rest of the paleocanyon fill by granitic basement, so its stratigraphic position is not known (Fig. 2). It is, however, clearly intruded on its southeast margin by the basaltic andesite of Round Top (Fig. 2), which has a K/Ar date of 13.4 ± 1.5 Ma (Armin et al., 1984), providing a minimum age on the section. Because there is no maximum age control on the Elephant's Back section, it could be older than the other units shown in sequence 1 (Fig. 2B).

The volcanic lithic sandstones and breccia conglomerates of Elephant's Back are finer grained, better sorted, and better rounded than other map units at Carson Pass. Although dominated by andesite clasts, the Elephant's Back units also contain more mafic and hypabyssal (holocrystalline) clasts than other map units at Carson Pass (Table 1). This may indicate a more distal and diverse, somewhat dissected, volcanic source relative to other units at Carson Pass.

Basaltic Andesite Intrusions of Round Top (Tbai)

The basaltic andesite intrusions of Round Top and nearby areas (Tbai) are interpreted to be a subvolcanic intrusion, presumably exposed by erosion of an overlying volcanic edifice. It contains distinctive large hornblende glomerocrysts, locally in clots as large as tens of centimeters, and resorbed plagioclase, suggesting a complex magmatic history (Table 1).

The K/Ar date of 13.4 ± 1.5 Ma reported by Morton et al. (1977) was from a sample collected on the southern tip of Elephant's Back (Fig. 2). The K/Ar age is thus coeval (within error) with the sequence 2 trachyandesite block and ash flow tuff of Carson Pass (Taba1). Furthermore, whole-rock X-ray fluorescence data from one of the sequence 2 debris-flow deposits at Castle Point (Tfdf), presented in the GSA Data Repository, indicates the presence of at least one basaltic andesite block that is chemically similar to the basaltic andesite intrusion of Round Top (Tbai). For these reasons, we tentatively place the basaltic andesite intrusions of Round Top in sequence 2 (Fig. 2). However, the error on the K/Ar date is too large to know whether the Round Top intrusion (Tbai) is older, younger, or the same age as the Carson Pass block and ash flow tuff (Taba1).

Sequence 3

Unconformity 3 (Fig. 2) underlies the most widespread units in the Carson Pass–Kirkwood Valley area, which are the lower, poorly sorted fluvial unit (Tfl) and the upper, well-sorted fluvial unit (Tfu). The unconformity is steepest where it is cut into sequence 2, both at the west end of the field area along Highway 88 (Figs. 2 and 3A), and at the east end of the field area, where it forms two buttresses against the trachyandesite block and ash flow tuff and debris-flow deposits of Carson Pass (Taba1) (Figs. 4B and 3D). The unconformity slopes more gently where it is cut into granite (Fig. 3B, 4A, and 4C), but is stepped in longitudinal view of the paleocanyon (Fig. 4A). The maximum vertical relief on this surface is 315 m, its maximum gradient is 6°, and it can be traced across the width of the 7–8-km-wide paleocanyon (Fig. 3), as well as 18 km down the paleocanyon axis (Fig. 2).

Lower Fluvial Deposits (Tfl), Reworked Pumice Lapilli Tuff (Trt), and Upper Fluvial Deposits (Tfu)

Both the lower and upper fluvial deposits (Tfl, Tfu) are well-stratified, clast-supported breccia conglomerate and pebbly sandstone, composed of a variety of intermediate-composition volcanic clasts. These units are interpreted as braided stream deposits (see footnote 1). Both are readily distinguishable from all other map units by their lack of interstratified volcanic debris-flow deposits or primary volcanic deposits. They thus probably record a local hiatus in eruptive activity. The lower fluvial deposit, which is a slope former, is coarser and less well sorted than the upper fluvial deposits, which are cliff-formers. We could not systematically collect paleocurrent data for these units because they are dominantly planar-stratified (rather than cross-stratified), and most clasts are too round to show imbrication; however, clast imbrication, wherever present, consistently indicates transport toward the southwest to west (Fig. 2), as does alignment of logs at the base of the upper fluvial unit (see Data Repository). The dominance of andesitic volcanic clasts in these deposits and the transport direction suggest an active andesitic source to the east of Carson Pass during accumulation of this unit, the age of which is between 14.69 ± 0.06 (sequence 2) and 10.49 ± 0.12 Ma (sequence 5).

The reworked pumice lapilli tuff (Trt) fills a small channel cut into the top of the lower fluvial unit (Tfl) and is overlain by the upper fluvial unit (Tfu) on Little Round Top Ridge (Fig. 2). This unit is enigmatic because in the field and in thin section it appears to be a primary pyroclastic deposit, but age data show that it is not.

In outcrops it is a clean, white, unsorted, massive pumice lapilli tuff, and in thin section the matrix is dominated by bubble-wall shards and euhedral sanidine and quartz crystals (Table 1). The matrix also contains minor volcanic rock fragments, but they are welded ignimbrite, a feature that may occur in primary pyroclastic flow deposits. We considered it a distal pyroclastic flow deposit and expected that $^{40}\text{Ar}/^{39}\text{Ar}$ dating of the sanidines in it would closely delimit the ages of the enclosing fluvial units. Instead, the sanidines yield a mixture of late Oligocene ages (Table 2) that are clearly much older than the strata we have dated downsection from this unit (Fig. 2B). The delicate nature of pyroclastic material is in general used to infer penecontemporaneous volcanism; such material is widely regarded to be able to survive temporary storage and resedimentation, but not long-term storage, which involves destructive processes like lithification and alteration. Nonetheless, this unit appears to be composed of delicate pyroclastic material that was erupted in the Oligocene and reworked ~8–12 m.y. later, in the middle Miocene.

Sequence 4

Unconformity 4 only occurs on the east side of the Kirkwood Valley (Fig. 2), where the fluvial units of sequence 3 (Tfl and Tfu) are deeply incised, forming a paleocanyon wall (Figs. 3B, 4C, and 4D). The maximum vertical relief on unconformity 4 is 227 m, with a paleoslope gradient of 32° and a lateral extent of 1.4 km (Fig. 3).

Andesite Block and Ash Flow Tuff of East Kirkwood (Taba2)

The andesite block and ash flow tuff of east Kirkwood Valley (Taba2) is a vent-proximal deposit that indicates a return of volcanism to the Carson Pass region after the local volcanic hiatus of sequence 3. This unit is preserved as erosional remnants between unconformity 4 below and unconformities 5 and 6b above (Figs. 2, 3B, 4C, and 4D). Like all the other primary volcanic strata below sequence 6, it contains abundant hornblende (Fig. 8).

Sequence 5

Unconformity 5 is in the western half of the map area, around Kirkwood Valley (Fig. 2), where it cuts down through sequences 3 and 2 to granitic basement (Figs. 3A, 3B, 4A, 4C, and 4E). The maximum vertical relief on sequence boundary 5 is 200 m, with a maximum paleoslope gradient of 32° and a lateral extent of 4.2 km (Fig. 3). This very deep unconformity is referred to as reincision 2 (Fig. 10D).

Volcanic Debris-Flow Deposits of Kirkwood (Tvdf1) and Interstratified Lava Domes (Tad1, Tad2)

The volcanic debris-flow deposits of Kirkwood (Tvdf1) form a section as much as 300 m thick (Figs. 3A and 4). We have not yet found a way to distinguish it lithologically from a demonstrably younger map unit, the volcanic debris-flow deposits of Little Round Top (Tvdf2). The volcanic debris-flow deposits of Kirkwood contain blocks as long as tens of meters (Table 1), suggesting a proximal source area for the volcanic debris flows. The volcanic debris-flow unit also contains hyperconcentrated flood-flow deposits, which differ from the debris-flow deposits mainly by being somewhat better stratified. These are at the top of section around Thimble Peak (Fig. 2), where they appear to have slumped into a very broad shallow channel cut into the top of the debris-flow section (see photomosaic in DeOreo, 2004).

The volcanic debris-flow deposits of Kirkwood (Tvdf1) are interstratified with andesite shallow-level intrusions that pass upward and outward into lava dome, dome breccia, and associated tuffs (Tad1 and Tad2, Fig. 2; Table 1). These record volcanism within the paleocanyon as it filled. The volcanic debris-flow deposits of Kirkwood (Tvdf1) are also cut by the 10.49 ± 0.12 Ma andesite dike with peperite margins (Figs. 5H, 5I; Table 1). This dike was therefore intruded while the debris-flow deposits were still unconsolidated and saturated with water; thus, we consider it penecontemporaneous with the volcanic debris-flow deposits of Kirkwood (Tvdf1). We expected the peperite dike (and the debris-flow deposits it intrudes) to be the same age as the sequence 6 volcanic rocks, because, like those pyroxene-bearing units, it lacks hornblende (peperite dike of east Kirkwood, Fig. 8). This led us initially to correlate the debris-flow deposits of Kirkwood (Tvdf1, sequence 5) with those of Little Round Top (Tvdf2, sequence 6a, Fig. 2). However, the peperite dike is ~4 m.y. older than primary volcanic rocks of sequence 6, so the two otherwise indistinguishable debris-flow deposits are quite different in age (Fig. 2B).

Sequence 6

We divide unconformity 6 into unconformities 6a and 6b because of geographic separation; 6a is restricted to the eastern half of the map area and 6b is in the western half of the map area, so unconformities 6a and 6b cannot be mapped continuously into each other (Fig. 2A), although they are probably correlative. Similarly, sub-sequences 6a and 6b probably record related volcanism (Figs. 2B and 8). The strata directly overlying unconformities 6a and 6b are similar

in age, the basal strata of sequence 6a being between 0.75 and 1.1 m.y. older than the basal strata of sequence 6b (Table 1). The block and ash flow tuffs at the tops of both sequences 6a and 6b (Taba3 and Tbat, Fig. 2) are petrographically and geochemically similar (Fig. 8; see data repository); if they are proven correlative by future work (e.g., trace element geochemical studies or $^{40}\text{Ar}/^{39}\text{Ar}$ dating of unit Tbat), then sequences 6a and 6b could be combined into a single sequence (sequence 6).

Unconformity 6 represents a third very deep unconformity within the paleocanyon, referred to as reincision 3 in Figure 10F.

Sequence 6a

On Little Round Top ridge, unconformity 6a forms a gently sloping surface (Fig. 4A), but at least 6 m.y. is not represented across that contact, using the age brackets on the sequence 3 upper fluvial unit (Tfu) below the unconformity and the age of the sequence 6 basalt lava flows (Tbl) above the unconformity (Fig. 2B; Table 1). On Red Lake Peak ridge, unconformity 6a cuts into the upper fluvial unit (Fig. 3D), as well as the sequence 2 trachyandesite block and ash flow tuff (Taba1), and the basalt lava flows lap out eastward against this cut (Figs. 2 and 4B). Unconformity 6a has a maximum vertical relief of 303 m, a maximum gradient of 48°, and a lateral extent of 6.0 km (Fig. 3).

Basalt Lava Flows of Carson Pass (Tlb)

Black, glassy, aphyric or olivine- and plagioclase-phyric basalt lava flows are easily distinguishable from other map units (Table 1). At least four flows are present, separated by flow breccia or vesicular flow tops. One aphyric basalt lava flow from Little Round Top ridge is dated as 6.80 ± 0.20 Ma (Figs. 2 and 9G; Table 1).

Volcanic Debris-Flow Deposits of Little Round Top (Tvdf2)

The volcanic debris-flow deposits of Little Round Top (Tvdf2) are lithologically indistinguishable from those of the volcanic debris flows of Kirkwood (see Tvdf1, sequence 5; Table 1). These deposits can only be discriminated on the basis of geochronological evidence (Table 1); i.e., the volcanic debris flows of Kirkwood (Tvdf1) are cut by a 10.50 ± 0.12 Ma peperite dike, and the volcanic debris-flow deposits of Little Round Top (Tvdf2) overlie a 6.80 ± 0.20 Ma basalt lava flow (Tbl).

Basaltic Andesite Block and Ash Flow Tuff of Red Lake Peak (Tbat)

This block and ash flow tuff forms the summit of the highest point within the paleocanyon,

Red Lake Peak (Figs. 2, 3D, and 4B). Like the 6.05 ± 0.12 Ma andesite block and ash flow tuff of the Sentinels (Taba3), the basaltic andesite block and ash flow tuff of Red Lake Peak (Tbat) contains, at most, trace amphibole (Fig. 8). This similarity, and the fact that both of these deposits occupy the highest stratigraphic positions in their respective parts of the map area (Fig. 2), suggests that these block and ash flow tuffs could be approximately time equivalent. This would support the conclusion that the ~170-m-thick volcanic debris-flow deposits of Little Round Top were deposited in <0.75 m.y., but further geochronology (i.e., a date on the basaltic andesite block and ash flow tuff of Red Lake Peak; Tbat) is needed to confirm this hypothesis.

Sequence 6b

Unconformity 6b is relatively flat on most of the length of west Kirkwood ridge (Fig. 4E), except for its westernmost end (Fig. 4A), and it cuts steeply down through sequences 5 and 4 on east Kirkwood ridge (Figs. 4C, 4D). This sequence boundary has a maximum vertical relief of 303 m, a maximum paleoslope gradient of 6° , and a lateral extent of 5.0 km (Fig. 3)

Andesite Block and Ash Flow Tuff of the Sentinels (Taba3)

This block and ash flow tuff contains abundant bread-crust and prismatically jointed blocks. On Melissa Coray Peak, where it was deposited on granitic basement, some of the meter-scale blocks in the deposit have elongate (10 cm) striations developed on the surface of an ~1 cm-thick layer of homogeneous black glass. These are interpreted as friction marks similar to those observed in andesite block and ash flow tuffs erupted from the Soufriere Hills volcano in Montserrat (Grunewald et al., 2000).

Modal analyses of block and ash flow tuffs and coherent intrusions from throughout the map area (Fig. 8) show that the andesite block and ash flow tuffs of the Sentinels are petrographically distinct from the other primary volcanic rocks of the area, with the exception of the basaltic andesite block and ash flow tuff of Red Lake Peak. The andesite block and ash flow tuff of the Sentinels (Taba3) displays a conspicuous lack of amphibole (except as resorbed or reacted xenocrysts present in trace amounts), and the basaltic andesite block and ash flow tuff of Red Lake Peak is the only other map unit with this characteristic. We thus tentatively correlate them. The andesite block and ash flow tuff of the Sentinels is dated as 6.05 ± 0.12 Ma (Table 1), and is the highest stratigraphic unit in the western part of the map area.

Rocks of Unknown Age

Rocks of Black Butte (Fig. 2) are described in the GSA Data Repository (see footnote 1), but they cover a very small area and are undated, so they are not discussed further.

GEOCHRONOLOGY

Analytical Methods

Standard density and magnetic separation techniques were used to generate separates. Separates were irradiated in a cadmium-lined tube at the TRIGA reactor at Oregon State and were analyzed in the $^{40}\text{Ar}/^{39}\text{Ar}$ geochronology laboratory at the University of California Santa Barbara using the general procedures and system described by Gans (1997). The flux monitor used for all irradiations was Taylor Creek Rhyolite with an assigned age of 27.92 Ma (Duffield and Dalrymple, 1990). For comparison, we obtained an age of 27.60 Ma on Fish Canyon Tuff Sanidine. All errors given for our estimated (preferred) ages as reported throughout the text, and in Table 2 are estimated $\pm 2\sigma$ (95% confidence), whereas error bars and uncertainties quoted on the spectra (Fig. 9) are 1σ . Some of the ages and uncertainties listed in Table 2 are rounded from the original calculated ages to the estimated most significant digit. In general, weighted mean plateau ages (WMPA, defined as the weighted mean age of 2 or more contiguous steps, and usually representing more than 50% of the total gas released) and uncertainties are reported, rather than the associated inverse isochron ages, though in all cases they are within error of each other. Complete data tables, age spectra, inverse isochron plots, K/Ca spectra, and further analytical details for all of the samples analyzed are provided in the GSA Data Repository.

Interpretation of Results

Most samples produced well-behaved data with readily interpretable ages. Plagioclase and biotite generally yielded fairly flat age spectra with concordant plateau and inverse isochron ages for large fractions of the gas released (Table 2; Fig. 9; Data Repository). Whole-rock results (groundmass concentrates) from two of the samples (CP-20 WR, CP-62 WR) are more complex (Table 2; Figs. 9E, 9G). The shapes of these spectra and their deviation from an idealized flat plateau are readily explainable in terms of the combined effects, but variable contributions of reactor-induced recoil, low-temperature argon loss, and a nonatmospheric trapped component (i.e., excess argon). In general, the flattest and most reliable parts of the whole-rock

spectra are associated with the gas released at intermediate to high temperatures (e.g., Gans, 1997). The plateau segments for these spectra represent only 20%–35% of the gas released, and thus these interpreted ages are of somewhat lower reliability. In cases where the individual steps in this segment are not within 2σ analytical uncertainty of each other, we assign an uncertainty corresponding to one standard deviation of the selected ages; this is a somewhat arbitrary assessment, but one that has proven conservative where independent age constraints exist.

Our new $^{40}\text{Ar}/^{39}\text{Ar}$ geochronologic data show that volcanic activity in Carson Pass spanned from at least 14.69 ± 0.06 Ma to 6.05 ± 0.12 Ma (Table 2; see following for detailed description of results for each sample). The K/Ar age of 5.2 ± 0.8 Ma from Stevens Peak (Fig. 2A) (Armin et al., 1984) comes from an andesite intrusion that is too propylitized to be suitable for future $^{40}\text{Ar}/^{39}\text{Ar}$ dating. The basaltic andesite block and ash flow tuff of Red Lake Peak (Fig. 2) is a better candidate for determining the age of youngest volcanic activity in this area because it is fresh and well exposed, and because it unequivocally occupies the highest point in the local stratigraphy.

Trachyandesite Block and Ash Flow Tuff of Carson Pass (Taba1)

Incremental heating results from plagioclase and biotite from this sample yielded generally concordant results, the biotite providing the far more precise age. The biotite yields slightly older ages for low-temperature steps, but flattens at higher temperatures to yield a well-defined plateau age (WMPA) of 14.69 ± 0.06 Ma (Fig. 9B) and an isochron age of 14.73 ± 0.62 Ma for the last 76% of the gas released (3 steps). The associated plagioclase had low radiogenic yields and inconsistent K/Ca ratios (see Data Repository), but yields an acceptable WMPA of 14.1 ± 0.7 Ma (Fig. 9A) and isochron of 13.25 ± 1.75 Ma, both within error of the biotite result.

Reworked Pumice Lapilli Tuff (Trt) between Lower and Upper Fluvial Deposits (Tfl and Tfu)

Sanidine was analyzed from this reworked deposit in an attempt to establish a maximum depositional age. A conventional incremental heating experiment on a bulk separate of sanidine yielded a disturbed spectrum with single step ages that climbed monotonically from 23.3 to 24.0, yielding an integrated total fusion age of 23.64 Ma, but with no meaningful plateau or inverse isochron age (Fig. 9D; see data repository). Five total fusion experiments on single grains and small groups of grains are plotted by increasing age as a spectrum in Figure 9C, with

each step reflecting a separate fusion. The first three steps represent single sanidine grains and yield ages of 22.9 ± 0.1 , 23.2 ± 0.1 , and 23.2 ± 0.1 Ma. The last two steps represent fusions of several grains and yielded concordant ages of 23.4 ± 0.1 Ma. These data suggest that the lapilli tuff contains at least three populations of sanidine with ages of 22.9 Ma, 23.2 Ma, and older than 24 Ma, and that the maximum depositional age for this unit can be no older than 22.9 ± 0.1 Ma.

Peperite Dike in Volcanic Debris-Flow Deposits of Kirkwood (Tvd1)

Whole-rock (groundmass concentrate) and plagioclase separates of the andesite dike with peperite margins were analyzed, the plagioclase providing the more reliable result. The whole-rock sample yielded a disturbed spectrum that is typical of reactor-induced recoil with no clear plateau or isochron age, and apparent ages that decrease monotonically from 12.0 to 10.3 Ma (Fig. 9E). A reasonable assessment of the age for this sample is provided by the mean age of 10.6 ± 0.2 Ma for the 23% of the gas released in the 920 to 1200 °C steps (Fig. 9E; Table 2). Though this short, flat segment of the spectra constitutes only a small portion of the total gas released, the estimated age is concordant with the results obtained from plagioclase from the same unit. The plagioclase yielded a well-defined plateau for 89% of the gas released (Fig. 9F), with a calculated WMPA of 10.49 ± 0.12 and concordant isochron age of 10.48 ± 0.20 (see GSA Data Repository).

Basalt Lava Flow of Carson Pass (Tb)

A whole-rock (groundmass) sample of the basalt lava of Carson Pass also yielded a disturbed spectrum that is typical of reactor-induced recoil with no clear plateau or isochron age and apparent ages that decrease monotonically from ca. 10.0 to 6.5 Ma (Fig. 9G). A reasonable assessment of the age for this sample is provided by the mean age of ca. 6.8 Ma for the ~40% of the gas released in the 750 to 920 °C steps (Fig. 9G; Table 1). We assign an estimated uncertainty of ± 0.2 m.y. to the age of this sample (1 standard deviation of the selected step ages) to reflect the fact that no statistically meaningful plateau or isochron was obtained, even though the most reliable 50% of the spectrum is within these error limits.

Andesite Block and Ash Flow Tuff of the Sentinels (Taba2)

Plagioclase from the Sentinels block and ash flow tuff yielded an excellent flat spectrum (Fig. 9H), with concordant plateau and isochron ages of 6.05 ± 0.12 Ma and 5.99 ± 0.24 Ma for 100% of the gas released.

DISCUSSION

Ancestral Cascades Arc

The volcanic stratigraphy of the Carson Pass–Kirkwood paleocanyon is the result of two regional-scale magmatic episodes. First, the ca. 31–23 Ma ignimbrite flare-up swept southward across the Great Basin in Eocene–middle Miocene time (Christiansen et al., 1992; Wernicke, 1992; Humphreys, 1995). These ignimbrites were erupted from calderas in central Nevada and deposited in paleovalleys in western Nevada and eastern California (Garside et al., 2002, 2005; Faulds et al., 2005a). Second, the ca. 22–5 Ma ancestral Cascades erupted dominantly andesitic to dacitic, mostly effusive volcanic rocks in western Nevada and eastern California (Christiansen et al., 1992; Saucedo and Wagner, 1992; Garside et al., 2000, 2003). The third important regional magmatic episode, ca. 13 Ma to present, which is bimodal volcanism related to Basin and Range extension, is not represented in the fill of the Carson Pass–Kirkwood paleocanyon; instead, our geochemical and petrographic data show that this paleocanyon fill, and other paleocanyon fills of the central Sierra Nevada, were erupted in a continental volcanic arc setting (Fig. 8; GSA Data Repository; Busby et al., 2007).

Previous workers have drawn the boundaries of the ancestral Cascades arc in a swath that includes the central and northern Sierra Nevada as well as adjacent Nevada (Fig. 1A; Brem, 1977; Christiansen et al., 1992; Dickinson, 1997). Plate tectonic reconstructions for the location of the Mendocino triple junction (Atwater and Stock, 1998) suggest that subduction-driven volcanism could have continued in the latitude of the central Sierra Nevada until ca. 6–10 Ma. However, the exact location, age, and even the existence of a discrete band of subduction-related volcanism in the Miocene is somewhat unclear. This is because many andesites in the Sierra Nevada block of California and adjacent parts of the Basin and Range in Nevada remain unmapped and undated.

Outside the Sierra Nevada block in Nevada, andesites range in age from early Oligocene to late Miocene (e.g., Trexler et al., 2000; Garside et al., 2005). These rocks include the Wassuk Group of west-central Nevada (Golia and Stewart, 1984), 32 Ma andesites in central Washoe County (Bonham, 1969), 28 Ma andesite in the Carson Range (Garside et al., 2005), basaltic andesites that underlie ca. 27 Ma ignimbrites near Yerington (Proffett and Proffett, 1976), 20–23 Ma andesite, dacite, and rhyolite in the northern Pah Rah–southern Virginia Mountains (Garside et al., 2003; Faulds et al., 2005b),

15.5 Ma Upper Alta andesite, 14.5 Ma Kate Peak Formation, and ca. 12 Ma intermediate volcanic rocks in the Comstock district of Nevada (Castor et al., 2002; Chris Henry, 2006, personal commun.). Andesitic volcanism as young as ca. 5 Ma has been recognized in western Nevada (John et al., 1999).

In the Sierra Nevada block, in contrast, andesite volcanism appears to be largely restricted to the middle and late Miocene. Our new $^{40}\text{Ar}/^{39}\text{Ar}$ ages, taken together with mostly K/Ar ages reported from the literature, allow us to speculate that three pulses of calc-alkaline andesite volcanism may have occurred in the Miocene (although more data are needed): ca. 15–14 Ma, 10–9 Ma, and 7–6 Ma. The oldest andesite volcanic rocks within the Sierra Nevada block appear to be middle Miocene, or ca. 15 Ma, with the exception of an andesite lava flow in the Carson Range dated as 28 Ma (Garside et al., 2005). The 15.4 Ma Lovejoy basalt is the oldest Tertiary volcanic rock demonstrably vented within the Sierran block, and it is the largest eruptive unit identified in California, but it is unrelated to volcanism of the predominantly calc-alkaline Cascade arc. Instead, the Lovejoy is a quartz-normative tholeiite, with major and trace element characteristics similar to the 6.5–15 Ma Grande Ronde flows of the Columbia River Group (Garrison, 2004). We interpret the Lovejoy basalt to record rapid migration of plume head material, at ~20 cm/yr, to the southwest, in a direction not previously recognized (Garrison et al., 2007). It erupted in front of the locus of arc magmatism, which was to the east in Nevada. The Lovejoy Basalt is overlain by a 14.0 ± 0.5 Ma plagioclase andesite block and ash flow tuff, which is overlain by a 9.96 ± 0.13 Ma hornblende andesite block and ash flow tuff (new $^{40}\text{Ar}/^{39}\text{Ar}$ ages reported in Garrison, 2004; Garrison et al., 2007). These ages are similar to the first two pulses of magmatism in the Carson Pass–Kirkwood paleocanyon, described here (14.69 ± 0.06 Ma and 10.49 ± 0.12 Ma). The older age is also represented by a clast within an andesitic debris-flow deposit at Oroville Table Mountain (northern Sierra Nevada), dated as 14.38 ± 0.29 Ma by K/Ar (Wagner and Saucedo, 1990). The Oroville section contains an anomalously old, coarse-grained, well-rounded, andesite-clast conglomerate (David Wagner, 2006, personal commun.); it is overlain by a dacitic tuff dated as 24.4 Ma by K/Ar (Dalrymple, 1964; recalculated in Wagner and Saucedo, 1990), and related as 24.69 ± 0.71 Ma by K/Ar on sanidine (Wagner and Saucedo, 1990). The source of this andesitic detritus is not known, but is likely in Nevada.

The younger (ca. 10 Ma) early-late Miocene pulse recorded at Carson Pass is also represented

in the northern Sierra Dixie Mountain area, which we interpret to represent an eroded Christmas-tree laccolith that locally pierced its cover (Roulet et al., 2005; Roulet, 2006). The laccolith intrudes a section of volcanic debris-flow deposits and interstratified block and ash flow tuffs dated as 10.85 ± 0.2 Ma, and the ages of three samples from the intrusive to extrusive parts of the complex overlap within error at $10.5\text{--}10.4 \pm 0.2$ Ma ($^{40}\text{Ar}/^{39}\text{Ar}$ ages reported in Roulet, 2006). The younger (early-late Miocene) pulse of calc-alkaline volcanism is also very well represented by 10.10 ± 0.06 Ma andesitic block and ash flow tuffs and 10.35 ± 0.25 Ma andesite dikes in the Sonora Pass area of the central Sierra Nevada; this pulse was immediately followed by voluminous high-K volcanism at 10.25 ± 0.06 Ma to 9.16 ± 0.03 Ma ($^{40}\text{Ar}/^{39}\text{Ar}$ ages reported in Busby et al., 2007). Evidence for the older (ca. 14–15 Ma) pulse of volcanism has not yet been found at Sonora Pass.

The youngest, ca. 6–7 Ma pulse of volcanism represented by lava flows, block and ash flow tuffs, and peperite complexes at Carson Pass is also well represented by intrusions and vent-proximal volcanic rocks in the Sonora Pass to Ebbetts Pass area of the central Sierra (summarized by Busby et al., 2007).

Our new work shows that in general, Miocene eruptive centers were sited along the modern Sierran range crest in the Carson Pass–Kirkwood area, as well as in other parts of the central Sierra. These centers built lava domes that collapsed to generate block and ash flow tuffs, which in turn were remobilized down-canyon to produce volcanic mudflow and minor dilute-flow (stream) deposits.

We find no evidence for large volcanic centers such as the eroded remnants of large stratovolcanoes or calderas; instead, vent facies consist of relatively small andesite hypabyssal intrusions, dikes, and sills, and vent-proximal facies consist largely of small andesite lava domes that collapsed to produce block and ash flows, and minor andesite lava flows. Lava flows are rare; instead, magmas invaded wet volcanoclastic sediment to form *in situ* peperite piles that were partly remobilized to form debris flows or block and ash flows with peperite domains. We interpret the following lithofacies to reflect vent- and vent-proximal volcanism in the Carson Pass–Kirkwood Valley area: subvolcanic intrusions, *in situ* peperites, dikes, plugs, domes, dome breccias, and block and ash flow tuffs. These occur in sequences 2, 4, 5, and 6 (Fig. 2).

Other lithofacies are considered to record deposition at sites medial to distal from Miocene volcanic centers. These include volcanic debris-flow deposits, volcanoclastic hyperconcentrated flood-flow deposits, and volcanoclas-

tic fluvial deposits (sequences 2, 3, 5, and 6). Nearly all of the debris-flow and fluvial units contain abundant angular to subangular blocks, suggesting that they were deposited at sites relatively close to their volcanic sources, and they generally lack fine-grained horizons, suggesting deposition on relatively steep slopes. The only exception to this is the siltstone, sandstone, pebbly sandstone, and cobble breccia conglomerate of Elephant's Back (Tsb and Tvs, sequence 2, Fig. 2). The fluvial deposits are also nearly all bouldery, suggesting deposition from high-gradient braided streams.

This study also demonstrates that the interaction of andesitic magma and wet clastic deposits and the consequent generation of peperite was a common process during middle Miocene time near the crest of the Sierra Nevada in central California. We suggest that areas of active volcanism in fluvial montane environments are particularly favorable to peperite generation, and in particular to its incorporation as domains or clasts in subsequent fluvial and volcanic deposits. This is because such volcanic environments are characterized by both high rates of erosion and clastic deposition in a wet setting. Andesitic peperite has been described (Branney and Suthren, 1988; Brooks et al., 1982; Doyle, 2000; Goto, 1997; Hanson, 1991; Hanson and Hargrove, 1999; Kano, 1989, 1991, 1998, 2002; Kokelaar, 1982; Snyder and Fraser, 1963; Williams, 1929; Williams and Curtis, 1977), but none of these descriptions are of peperite associated with coarse volcanic and sedimentary deposits in fluvial montane settings. Peperite generation in fluvial montane environments has implications for process recognition and hazards associated with many andesitic volcanoes. The recognition of peperite requires careful examination to distinguish it from very similar coarse rocks of both volcanic and sedimentary origin (Skilling et al., 2002), and many examples may have been overlooked or misinterpreted; descriptions given here are useful for aiding future workers in recognizing them. The Mehrten Formation peperite-bearing deposits demonstrate that the generation of a peperitic carapace should be considered when modeling slope and/or edifice stability related to high-level intrusion, particularly in areas of high rates of sedimentation.

Landscape Evolution

Early workers concluded that almost all of the present-day topography in the Sierra Nevada range was created by late Cenozoic uplift (Lindgren, 1911; Ransome, 1898), but later workers made a distinction between basement topography and river canyons that have been rapidly incised since the Pleistocene (e.g., Bateman

and Wahrhaftig, 1966; Huber, 1981; Stock et al., 2004). Paleorelief in the Sierra Nevada is defined as relief that predates late Cenozoic deposits and can be determined by comparing the elevation of local basement highs to the local base of Cenozoic strata (Fig. 10H; Bateman and Wahrhaftig, 1966; Wakabayashi and Sawyer, 2001). Our mapping shows that paleorelief in the Carson Pass–Kirkwood area is ~650 m. This matches paleorelief calculations for nearby basement high peaks: 660 m at Pyramid Peak to the north and 680 m at Mokelumne Peak to the southwest (Bateman and Wahrhaftig, 1966). This finding also agrees with Wakabayashi and Sawyer's (2001) observation of low (<200 m) paleorelief values in the northern Sierra Nevada, high values (>1000 m) in the southern Sierra, and intermediate values in the central part of the range. It might therefore be considered reasonable to estimate that absolute elevation in the Kirkwood–Carson Pass area ca. 5–10 Ma was between 900 m and 2500 m, based on the estimates for the northern and southern end of the range, respectively, by Wakabayashi and Sawyer (2001). This large-scale morphology, coupled with thermochronologic data from the northern and southern Sierra Nevada suggesting high exhumation rates in the Cretaceous followed by low rates throughout the Neogene, can be used to make arguments for the antiquity of the range (Cecil et al., 2006). Thermochronological data are completely lacking for the central Sierra. This paper makes use of geological data bearing on its landscape evolution.

A low-relief Eocene relict landscape has been identified in the southern Sierra Nevada, where Cenozoic strata are rare (Clark et al., 2005). This consists of low-relief upland surfaces developed on bedrock that trace northward into a low-relief nonconformity at the base of an Eocene–Miocene section along the western flank of the central Sierra Nevada (Clark et al., 2005). The low-relief Eocene surface has also long been recognized in the northern Sierra (Bateman and Wahrhaftig, 1966), where it was interpreted as a product of low-elevation planation (Huber, 1981). However, Cecil et al. (2006) point out that intense weathering may produce moderate- to low-relief surfaces independent of elevation, and that thick, deeply weathered paleosols in the northern Sierra indicate a tropical to subtropical climate in Eocene time (the torrid age). We propose that deep weathering of granitic basement during the Eocene could partly explain the almost total lack of granitic cobbles and boulders from Oligocene ignimbrites at the base of central and northern Sierra Nevada paleocanyons; perhaps they were weathered away. This suggestion is consistent with the fact that the Eocene conglomerates of the northern Sierra

and western central Sierra lack much granitic detritus, although they are clearly derived from within the range (Lindgren, 1911; Bateman and Wahrhaftig, 1966; David Wagner, 2006, personal commun.). Granites clearly weather more quickly than most other rock types, but the Eocene climate probably speeded this process.

We have identified neither the relict landscape of the southern Sierra nor the laterites of the northern Sierra in our studies of the crestral central Sierra Nevada. In the southern Sierra, the relict landscape is absent where it has been eroded away in canyons or by Pleistocene glaciers. Perhaps this means that the Eocene relict landscape has been entirely eroded away by glaciers in crestral areas of the central Sierra, despite inferred higher elevations in the south. This could perhaps be the result of a strong climatic gradient (Kurt Cuffy, 2006, personal commun.). However, this does not explain the lack of Eocene paleosols beneath the Oligocene rocks in the central Sierra; perhaps the paleosols were eroded, indicating that local relief and axial gradients in the paleocanyons were greater than previously envisioned.

We refer to the Carson Pass–Kirkwood paleocanyon as a paleocanyon, rather than paleovalley or paleochannel: this contrasts with Wakabayashi and Sawyer's (2001, p. 550–551) interpretation of low Tertiary stream gradients, referring to the "broad alluviated nature of the paleovalleys compared with narrow, bedrock-floored modern canyon (Bateman and Wahrhaftig, 1966; Christensen, 1966; Huber, 1981, 1990) ...consistent with low Eocene-Miocene incision rates." The Carson Pass–Kirkwood paleocanyon is not any broader than the modern canyons, and the paleocanyons in the central Sierra are steep-walled, with bouldery stream deposits, suggesting reasonably high axial gradients. Debris flows may move large clasts on low slopes, but streams do not. Our estimates of local relief are similar to those made by Clark et al. (2005) for the central Sierra Nevada; they estimated <500 m, and we estimate 650 m. However, our estimates of local slopes are much greater. Clark et al. (2005) estimated this as <10° for the central Sierra, whereas we map local slopes (maximum gradients of unconformities, Fig. 3) of up to 50° on granitic basement, to 70° on metamorphic basement, and to 48° on unconformities within the Tertiary paleocanyon fill. We also report somewhat deeper incisions within the Tertiary section than those reported by Wakabayashi and Sawyer (2001): they reported maximum Eocene–Miocene incision of 150 m, whereas we map multiple incision events of at least 200–300 m in the middle to late Miocene, and perhaps even more between the Oligocene and middle Miocene. We find no evidence, however, of widening or deep-

ening of the canyon into bedrock in Oligocene or Miocene time (Fig. 10).

In the central crestral Sierra, basal Oligocene ignimbrites are commonly preserved as thin erosional remnants on the deepest parts of the paleocanyon floors, but they originally formed canyon fills that became deeply incised before deposition of the middle Miocene andesitic volcanoclastic rocks (Figs. 10A, 10B). This contrasts with the northern Sierra Nevada, where ignimbrite paleocanyon fills did not get deeply incised in the Miocene, and in places the ignimbrites are also preserved outside the paleovalleys (Brooks et al., 2003; Garside et al., 2005). This supports the interpretation of Wakabayashi and Sawyer (2001) that the northern Sierra shows lower paleorelief than the central Sierra. It also may indicate that the central Sierra Nevada was affected by an early Miocene uplift event not evidenced in the northern Sierra.

For the ignimbrites to flow through channels all the way from central Nevada to the Sacramento Valley of California, surface elevations must have been higher in the Great Basin than the Sierra Nevada in Oligocene time. Wolfe et al. (1997) used paleobotanical evidence from western Nevada to infer high paleoelevations (3 km) at 15–16 Ma, and wrote that "the Sierra Nevada may have been no more than the western flank of the high plateau that constituted western Nevada" (p. 1674). The ignimbrites constitute geological evidence that this was the case for the Oligocene as well (Garside et al., 2005), and that the plateau rose at least as far east as central Nevada. This is consistent with paleobotanical and isotopic evidence for high elevations (2–3 km) of the Great Basin from the middle Eocene to the middle Miocene, summarized by Horton et al. (2004). Perhaps the clasts in the late Oligocene andesite conglomerate at Oroville Table Mountain came from central Nevada as well. Horton et al. (2004) also used the $\delta^{18}\text{O}$ and δD record of authigenic minerals to infer middle to late Miocene subsidence of the central Great Basin and southern Sierra (1–2 km) and central Sierra (700 m), during crustal extension. This leads to the question of the timing of beheading of the canyons that funneled pyroclastic flows across the Sierra Nevada.

Long before the Oligocene ignimbrites were correlated across the Sierra Nevada into central Nevada (Garside et al., 2005; Faulds et al., 2005a), workers recognized that chert pebbles in the Eocene auriferous gravels in the northern Sierra (Durrell, 1959) and at the base of the Miocene Mehrten Formation in the central Sierra (Bateman and Wahrhaftig, 1966) were derived from Paleozoic rocks of Nevada. Our detailed stratigraphic and geochronologic work provides constraints on the timing of disruption

of the upper reaches of the Nevada–eastern California paleochannels by Basin and Range faulting. There is geologic evidence that argues for beheading of the Carson Pass–Kirkwood paleocanyon by ca. 11 Ma. Sequence 3 (which is bracketed between 14.69 ± 0.06 Ma and 10.49 ± 0.12 Ma) has the most laterally extensive and thickest deposit in the paleocanyon (lower and upper fluvial units, Tfl and Tfu). Sequence 3 has the greatest volume of epiclastic rock, with a wide variety of andesite to basalt clast types, and it has no primary volcanic rocks, whereas all the other sequences do. Furthermore, it is the only sequence that lacks any catastrophically deposited debris flows. Instead, textures and sedimentary structures record streamflow, probably over a protracted period of time. Sequence 3 also has the reworked silicic ignimbrite with a probable ultimate source in western Nevada. For all of these reasons, we believe that the Carson Pass–Kirkwood paleocanyon described here was part of a much longer, persistent feature that was not beheaded until after deposition of sequence 3. This is consistent with the fact that paleocanyons of the Sonora Pass area in the central Sierra contain ignimbrites as young as 9.15 ± 0.03 Ma (Upper Member, Eureka Valley Tuff) that were erupted east of the present-day range crest (Busby et al., 2007).

We cannot determine the causes of the reincision events until we have more information from other central Sierra Nevada paleocanyons to determine whether they record local or regional events. Furthermore, thermochronologic data, which could provide constraints on the timing of uplift events, are completely lacking for the central Sierra, and our geologic results suggest that landscape evolution models developed for the southern and northern Sierra do not apply in detail to the central Sierra. As is true of all unconformities in the geologic record, possibilities for the causes of reincision events include tectonic uplift (or tilting), changes in climate or sediment supply, or changes in base level. All workers now agree that at least some (if not all) of the paleorelief in the range is inherited from the Cretaceous (our unconformity 1) and is tectonic in origin. However, we have documented three different ~300-m-deep unconformities within the paleocanyon fill (unconformities 2, 5, and 6, Figs. 2B and 3). These are probably too deep to be caused by eustatic base-level changes, and therefore may record tectonic or sediment supply changes. One possibility invoked for other volcanic terranes is eruption-induced aggradation, i.e., catastrophic sedimentation of pyroclastic flows, debris flows, and hyperconcentrated flood flows, triggered by the instant sediment supply of an explosively erupting volcano; this may be followed by dissection to base level (Smith, 1991).

However, there is no evidence for explosive eruptions in the Carson Pass–Kirkwood paleocanyon fill. Furthermore, the map unit with the largest volume, the lower and upper fluvial unit, is clearly not the product of catastrophic sedimentation. For these reasons, we interpret the three deep unconformities (2, 5, and 6) as recording tectonic events in the central Sierra Nevada.

We suggest that early Miocene tectonism in the central Sierra Nevada (reincision 1, Fig. 10B) may be related to the onset of arc magmatism there. Middle Miocene tectonism (reincision 2, Fig. 10D) could be related to Basin and Range extension, because our work in other parts of the central Sierra suggests that Basin and Range faulting began earlier there (by 10 Ma) than is envisioned for other parts of the Sierra (Busby et al., 2007). Late Miocene tectonism (reincision 3, Fig. 10F) may correspond to uplift attendant with the northward sweep of the triple junction through the latitude of the central Sierra. This is consistent with the fact that andesite volcanism ended in the latest Miocene (Fig. 10G), by 6 Ma (Fig. 2B). Alternatively, reincision 3 (Fig. 10F) could correspond to a second episode of faulting along the range front.

Sierran paleocanyons may make useful piercing points across Tertiary to Holocene faults (e.g., see Faulds et al., 2005a, b, and Garside et al., 2005, for the northern Sierra and adjacent Nevada). The central Sierra Nevada frontal fault zone has been interpreted to form a northwest-trending zone of en echelon escarpments produced by normal or oblique faulting (Wakabayashi and Sawyer, 2001; Schweickert et al., 2004), with focal plane mechanisms suggestive of oblique normal faulting (Unruh et al., 2003). The central Sierra Nevada frontal fault zone is at the western edge of the Walker Lane belt (Fig. 1A), which currently accommodates ~20%–25% of Pacific–North America plate motion (Bennett et al., 1999; Thatcher et al., 1999; Dixon et al., 2000; Oldow, 2000). We map the Carson Pass–Kirkwood paleocanyon eastward across the modern range crest through the Sierra Nevada frontal fault zone, where it bifurcates upstream into two tributaries (Busby et al., 2007). The paleocanyon shows normal offsets but no strike-slip offset, suggesting that long-term and short-term slip are not the same for this segment of the range-front fault system (Busby et al., 2007).

CONCLUSIONS

Previously undivided Tertiary strata of the Carson Pass–Kirkwood area, central Sierra Nevada, were mapped and dated with the goal of reconstructing the paleogeography of the ancestral Cascades arc and the evolution of the

Sierra Nevada landscape. Our main conclusions are the following.

1. The stratigraphy of the Carson Pass–Kirkwood paleocanyon records two regional-scale magmatic episodes, the Oligocene ignimbrite flare-up to the east in central Nevada, and middle to late Miocene andesitic effusive volcanism of the ancestral Cascades arc of the Sierra Nevada and parts of Nevada. These strata are preserved in a west-southwest-trending paleocanyon probably inherited from Cretaceous time, but reincised in early, middle, and late Miocene time.

2. Our new age data, together with published and unpublished age data presented here, allow us to propose that three phases of volcanism may have occurred in the ancestral Cascades arc in the Sierra Nevada: ca. 15–14 Ma (middle Miocene), 10–9 Ma (early-late Miocene), and 7–6 Ma (late Miocene). Miocene eruptive centers were sited along the modern Sierran range crest, and consist of small andesite hypabyssal intrusions that pass upward and outward into small andesite lava domes fringed by block and ash flow deposits. Lava flows are rare; instead, magmas invaded wet volcanoclastic sediment in paleocanyons to form *in situ* and resedimented peperites. Peperites have not been previously recognized in fluvial montane environments, but we believe they may be common and are important in considering hazards.

3. We interpret the floor and walls of the Carson Pass–Kirkwood paleocanyon to be a non-conformity cut into Mesozoic basement rock in Cretaceous time. Although we see no evidence of widening or deepening of the paleocanyon during deposition of late Oligocene–Miocene canyon fill, we map deep, high-gradient unconformities that may represent previously unrecognized tectonic events. The first event is represented by deep erosion of Oligocene ignimbrites in early Miocene time; this event may be restricted to the central Sierra Nevada, but we suggest that it is related to the onset of arc magmatism there. The second event is recorded by deep erosion of fluvial volcanoclastic rocks by ca. 10 Ma (middle Miocene), coinciding with the onset of range-front faulting in the central Sierra and beheading of the canyons that crossed it. This may have begun earlier in the central Sierra than it did in other parts of the range. The third event is recorded by reincision to bedrock in the late Miocene, just before the cessation of andesite volcanism at 6 Ma, and therefore may record uplift during triple junction passage, although a second episode of range-front faulting is also possible.

4. Although our new calculations of paleorelief support the interpretations of previous workers that the large-scale morphology of the

range has persisted since Cretaceous time, we find evidence for greater local paleorelief and higher axial paleogradients in the central Sierra than are predicted by previous workers in the northern and southern Sierra Nevada. This suggests that the Tertiary tectonic evolution of the range may vary along strike.

These interpretations can be tested by further mapping and dating of Tertiary strata and faults in the central Sierra, and by thermochronologic studies of the basement.

ACKNOWLEDGMENTS

Funding for this project was provided by National Science Foundation (NSF) grant EAR-0125179 (to Busby, Gans, and Skilling) and by the U.S. Geological Survey National Cooperative Geologic Mapping Program Awards 03HQAG0030 and 05HQAG0010 (to Busby). We thank Wanda Taylor, Patricia Cashman, and Terry Spell for very helpful formal reviews, and Jason Saleeby and Dave Wagner for informal reviews and many discussions.

We thank David Wagner for helping Busby and Skilling with the preparation of the NSF proposal that funded this work, for introducing us to the field area, and for his valuable feedback at all stages of the project, including supervision of Busby's Educational Mapping Program students Steve DeOreo and Jeanette Hagan. We also thank Keith Putirka for opening his lab to DeOreo and training him to collect geochemical data, and for helping with interpretation of the geochemical data, as well as for many helpful discussions with Busby in the field and office. We thank Martin Wong for his help with the $^{40}\text{Ar}/^{39}\text{Ar}$ geochronology, which included assisting DeOreo with sample selection and preparation, and also running the samples in the $^{40}\text{Ar}/^{39}\text{Ar}$ lab. We are grateful for field discussions with Brian Hausback, Chris Henry, Larry Garside, and Jim Faulds, as well as all 55 participants in the 2004 Volcanological Society of Sacramento field trip (list posted at: www.geol.ucsb.edu/faculty/busby). We acknowledge the Volcanological Society of Sacramento field trip honoree Garniss Curtis, who first mapped in this area more than 50 yr ago. Busby thanks Garniss Curtis for taking three hours to tell her all about the academic career path when she arrived at UC Berkeley as a junior college transfer student in September 1974.

REFERENCES CITED

- Armin, R.A., John, D.A., Moore, W.J., and Dohrenwend, J.C., 1984, Geologic Map of the Markleeville 15 Minute Quadrangle, Alpine County, California, Miscellaneous Investigations Series—U. S. Geological Survey, Report: I-1474, Department of the Interior, United States Geological Survey.
- Atwater, T., 1970, Implications of plate tectonics for the Cenozoic tectonic evolution of western North America: *Geological Society of America Bulletin*, v. 81, p. 3513–3536, doi: 10.1130/0016-7606(1970)81[3513:IOPTFT]2.0.CO;2.
- Atwater, T., and Stock, J., 1998, Pacific–North America plate tectonics of the Neogene southwestern United States—An update: *International Geological Review*, v. 40, p. 375–402.
- Axelrod, D.L., 1980, Contributions to the Neogene paleobotany of central California: University of California Press, 212 p.
- Bassett, K. and Busby, C., 2005, Structure and tectonic setting of an intra-arc strike-slip basin (Bisbee Basin, Southern Arizona), in Anderson, T.H., Nourse, McKee, J.A., J.W., and Steiner, M.B., eds., *The Mojave-Sonora megashear hypothesis: Development, assessment, and*

- alternatives: Geological Society of America Special Paper 393, p. 359–376.
- Bateman, P.C., and Wahrhaftig, C., 1966, Geology of the Sierra Nevada, in Bailey, E.H., ed., *Geology of northern California*: California Division of Mines Bulletin, v. 190, p. 107–172.
- Bennett, R.A., Davis, J.L., and Wernicke, B.P., 1999, Present-day pattern of Cordilleran deformation in the western United States: *Geology*, v. 27, p. 371–374, doi: 10.1130/0091-7613(1999)027<0371:PDPOCD>2.3.CO;2.
- Branney, M., and Suthren, R., 1988, High-level peperitic sills in the English Lake district: Distinction from block lavas, and implications for Borrowdale Volcanic Group stratigraphy: *Geology*, v. 23, p. 171–187.
- Brem, G.F., 1977, Petrogenesis of late Tertiary potassic volcanic rocks of the Sierra Nevada and western Great Basin [Ph.D. thesis]: Riverside, University of California, 361 p.
- Brooks, E.R., Wood, M.M., Boehme, D.R., Potter, K.L., and Marcus, B.L., 2003, Geologic map of the Haskell Peak area, Sierra County, California: California Geological Survey Map Sheet 55.
- Brooks, E.R., Wood, M.M., and Garbutt, P.L., 1982, Origin and metamorphism of peperite and associated rocks in the Devonian Elwell Formation, northern Sierra Nevada, California: Geological Society of America Bulletin, v. 93, p. 1208–1231, doi: 10.1130/0016-7606(1982)93<1208:OAMOPA>2.0.CO;2.
- Busby, C.J., and Bassett, K., 2007, Volcanic facies architecture of an intra-arc strike-slip basin, Santa Rita Mountains, Arizona: *Bulletin of Volcanology*, v. 70, no. 1, p. 85–103.
- Busby, C.J., Hagan, J.C., Putirka, K., Pluhar, C.J., Gans, P., Rood, D., DeOreo, S.B., and Skilling, I., 2008, The ancestral Cascades arc: Cenozoic evolution of the central Sierra Nevada (California) and the birth of the new plate boundary, in Wright, J.E., and Shervais, J.W., eds., *Ophiolites, Arcs, and Batholiths: Geological Society of America Special Paper 438*, doi: 10.1130/2008.2438(12) (in press).
- Busby-Spera, C.J., and White, J.D.L., 1987, Variation in peperite textures associated with differing host sediment properties: *Bulletin of Volcanology*, v. 49, p. 765–776, doi: 10.1007/BF01079827.
- Camus, G., Gourgaud, A., Moussand-Berthommier, P.-C., and Vincent, P.-M., 2000, Merapi (Central Java, Indonesia): An outline of the structural and magmatological evolution, with a special emphasis to the major pyroclastic events: *Journal of Volcanology and Geothermal Research*, v. 100, p. 139–163, doi: 10.1016/S0377-0273(00)00135-9.
- Castor, S.B., Garside, L.J., Henry, C.D., Hudson, D.M., McIntosh, W.C., and Vikre, P.G., 2002, Multiple episodes of magmatism and mineralization in the Comstock District, Nevada: Geological Society of America Abstracts with Programs, v. 34, no. 6, p. 185.
- Cecil, M.R., Ducea, M.N., Reiders, P.W., and Chase, C.G., 2006, Cenozoic exhumation of the northern Sierra Nevada, California, from (U-Th)/He thermochronology: *Geological Society of America Bulletin*, v. 118, p. 1481–1488.
- Chase, C.G., and Wallace, T.C., 1988, Flexural isostasy and uplift of the Sierra Nevada of California: *Journal of Geophysical Research*, v. 93, p. 2795–2802.
- Christensen, M.N., 1966, Late Cenozoic crustal movements in the Sierra Nevada of California: Geological Society of America Bulletin, v. 77, p. 163–182, doi: 10.1130/0016-7606(1966)77[163:LCCMIT]2.0.CO;2.
- Christiansen, R.L., Yeats, R.S., Graham, S.A., Niem, W.A., Niem, A.R., and Snively, P.D., Jr., 1992, Post-Laramide geology of the U.S. Cordilleran Region, in Burchfiel, B.C., et al., eds., *The Cordilleran orogen: Conterminous U.S.: Boulder, Colorado*, Geological Society of America, The geology of North America, v. G-3, 261–406.
- Clark, M.K., Maheo, G., Saleeby, J., and Farley, K.A., 2005, The non-equilibrium landscape of the southern Sierra Nevada, California: *GSA Today*, v. 15, p. 4–10, doi: 10.1130/1052-5173(2005)015[4:TNLOTS]2.0.CO;2.
- Curtis, G.H., 1951, The Geology of the Topaz Lake Quadrangle and the Eastern Half of the Ebbetts Pass Quadrangle. 1:125,000 [Unpublished Ph.D. thesis], University of California, Berkeley, 280 p.
- Curtis, G.H., 1954, Mode of origin of pyroclastic debris in the Mehrten Formation of the Sierra Nevada: University of California Publications in Geological Sciences, v. 29, p. 453–502.
- Dalrymple, G.B., 1963, Potassium-argon dates of some Cenozoic volcanic rocks of the Sierra Nevada: Geological Society of America Bulletin, v. 74, p. 379–390, doi: 10.1130/0016-7606(1963)74[379:PDOSCV]2.0.CO;2.
- Dalrymple, G.B., 1964, Cenozoic chronology of the Sierra Nevada, California: Los Angeles, University of California Press, 235 p.
- Davis, D.A., Henry, C.D., Garside, L.J., Faulds, J.E., and Goldstrand, P.M., 2000, Eocene-Oligocene paleovalleys cross the Sierra Nevada–Basin and Range boundary, western Nevada and eastern California: Geological Society of America Abstracts with Programs, v. 32, no. 6, p. 167.
- DeOreo, S., 2004, Volcanic and sedimentary history of the Carson Pass–Kirkwood paleoanion system: New geologic mapping, ⁴⁰Ar/³⁹Ar geochronology and geochemical analyses and their implications for the paleogeography of the Sierra Nevada Crest [M.S. thesis]: Santa Barbara, University of California, 135 p.
- Dickinson, W.R., 1997, Tectonic implications of Cenozoic volcanism in coastal California: Geological Society of America Bulletin, v. 109, p. 936, doi: 10.1130/0016-7606(1997)109<0936:OTIOCV>2.3.CO;2.
- Dixon, T.H., Miller, M., Farina, F., Wang, H., and Johnson, D., 2000, Present-day motion of the Sierra Nevada block and some tectonic implications for the Basin and Range province: North American Cordillera: *Tectonics*, v. 19, p. 1–24, doi: 10.1029/1998TC001088.
- Doyle, M.G., 2000, Clast shape and textural associations in peperite as a guide to hydromagmatic interactions: Upper Permian basaltic and basaltic andesite examples from Kiama, Australia: *Australian Journal of Earth Sciences*, v. 47, p. 167–177, doi: 10.1046/j.1440-0952.2000.00773.x.
- Ducea, M.N., and Saleeby, J.B., 1996, Buoyancy sources for a large, unrooted mountain range, the Sierra Nevada, California: Evidence from xenolith thermobarometry: *Journal of Geophysical Research*, v. 101, p. 8229–8244, doi: 10.1029/95JB03452.
- Ducea, M.N., and Saleeby, J.B., 1998, A case for delamination of the deep batholithic crust beneath the Sierra Nevada, California: *International Geology Review*, v. 40, p. 78–93.
- Duffield, W.A., and Dalrymple, G.B., 1990, The Taylor Creek Rhyolite of New Mexico; a rapidly emplaced field of lava domes and flows: *Bulletin of Volcanology*, v. 52, p. 475–487, doi: 10.1007/BF00268927.
- Durrell, C., 1959, The Lovejoy Formation of northern California: University of California Publications in Geological Sciences, v. 34, p. 193–219.
- Farmer, G.L., Glazner, A.F., and Manley, C.R., 2002, Did lithospheric delamination trigger late Cenozoic potassic volcanism in the southern Sierra Nevada, California: Geological Society of America Bulletin, v. 114, p. 754–768, doi: 10.1130/0016-7606(2002)114<0754:DLDTLC>2.0.CO;2.
- Faulds, J.E., Henry, C.D., and Hinz, N.H., 2005a, Kinematics of the northern Walker Lane: an incipient transform fault along the Pacific–North American plate boundary: *Geology*, v. 33, p. 505–508, doi: 10.1130/G21274.1.
- Faulds, J.E., Henry, C.D., Hinz, N.H., and Delwiche, B., 2005b, Transect across the northern Walker Lane, northwest Nevada and northeast California: An incipient transform fault along the Pacific–North American plate boundary, in Pederson, J., and Debie, C.M., eds., *Interior western United States: Geological Society of America Field Guide*, v. 6, p. 129–150.
- Fisher, R.V., and Heiken, G., 1982, Mt. Pelee, Martinique: May 8 and 20, 1902, pyroclastic flows and surges: *Journal of Volcanology and Geothermal Research*, v. 13, p. 339–371, doi: 10.1016/0377-0273(82)90056-7.
- Fisher, R.V., and Schminke, H.U., 1984, Pyroclastic rocks: Berlin, Springer Verlag, 472 p.
- Fisher, R.V., Smith, A.L., and Roobol, J.M., 1980, Destruction of St. Pierre, Martinique, by ash-cloud surges, May 8 and 20, 1902: *Geology*, v. 8, p. 472–476, doi: 10.1130/0091-7613(1980)8<472:DOSPMB>2.0.CO;2.
- Freundt, A., Wilson, C.J.N., and Carey, S., 2000, Ignimbrites and block and ash flow deposits, in Sigurdson, H., et al., eds., *Encyclopedia of volcanoes*: San Diego, California, Academic Press, p. 581–599.
- Gans, P., 1997, Large-magnitude Oligo-Miocene extension in southern Sonora; implications for the tectonic evolution of Northwest Mexico: *Tectonics*, v. 16, p. 388–408.
- Garrison, N., 2004, Geology, geochronology and geochemistry of the mid-Miocene Lovejoy flood basalt, northern California [M.S. thesis]: Santa Barbara, University of California, 65 p.
- Garrison, N.J., Busby, C.J., Gans, P.B., Putirka, K., and Wagner, D.L., 2008, A mantle plume beneath California? The Mid-Miocene Lovejoy flood basalt, northern California, in Wright, J.E., and Shervais, J.W., eds., *Ophiolites, Arcs, and Batholiths: Geological Society of America Special Paper 438*, doi: 10.1130/2008.2438(20) (in press).
- Garside, L.J., Castor, S.B., Henry, C.D., and Faulds, J.E., 2000, Structure, volcanic stratigraphy, and ore deposits of the Pah Rah Range, Washoe County, Nevada: Geological Society of Nevada Symposium 2000 Field Trip Guidebook No. 2, 132 p.
- Garside, L.J., Henry, C.D., and Boden, D.R., 2002, Far-flung ash-flow tuffs of Yerington, western Nevada erupted from calderas in the Toiyama Range, central Nevada: Geological Society of America Abstracts with Programs, v. 34, no. 6, p. 44.
- Garside, L.J., Castor, S.B., dePolo, C.M., and Davis, D.A., 2003, Geology of the Fraser Flat Quadrangle and the western half of the Moses Rock Quadrangle, Washoe County, Nevada, Map 146, Nevada Bureau of Mines and Geology.
- Garside, L.J., Henry, C.D., Faulds, J.E., and Hinz, N.H., 2005, The upper reaches of the Sierra Nevada auriferous gold channels, in Rhoden, H.N., Steininger, R.C., and Vikre, P.G., eds., *Geological Society of Nevada Symposium 2005: Window to the World*: Reno, Nevada, p. 209–235.
- Golia, R.T., and Stewart, J.H., 1984, Depositional environments and paleogeography of the upper Miocene Wasuk Group, west-central Nevada: *Sedimentary Geology*, v. 38, p. 159–180, doi: 10.1016/0037-0738(84)90078-2.
- Goto, Y., 1997, Interlayered sill-sediment structure at the base of a Miocene basaltic andesite sheet intrusion, Rebus Island, Hokkaido, Japan: *Journal of Mineralogy, Petroleum, Economic Geology*, v. 92, p. 509–520, doi: 10.2465/ganko.92.509.
- Grunewald, U., Sparks, R.S.J., Kearns, S., and Komorowski, J.C., 2000, Friction marks on blocks from pyroclastic flows at the Soufriere Hills volcano, Monserrat: Implications for flow mechanisms: *Geology*, v. 28, p. 827–830, doi: 10.1130/0091-7613(2000)28<827:FMOBFP>2.0.CO;2.
- Hamilton, W., and Myers, W.B., 1966, Cenozoic tectonics of the western United States: *Reviews of Geophysics*, v. 4, p. 509–549.
- Hanson, R.E., 1991, Quenching and hydroclastic disruption of andesitic to rhyolitic intrusions in a submarine island-arc sequence, northern Sierra Nevada, California: Geological Society of America Bulletin, v. 103, p. 804–816, doi: 10.1130/0016-7606(1991)103<0804:QAHDQA>2.3.CO;2.
- Hanson, R.E., and Hargrove, U.S., 1999, Processes of magma/wet sediment interaction in a large-scale Jurassic andesitic peperite complex, northern Sierra Nevada, California: *Bulletin of Volcanology*, v. 60, p. 610–626, doi: 10.1007/s004450050255.
- Heiken, G., and Wohletz, K., 1985, *Volcanic ash*: Berkeley, University of California Press, 246 p.
- Henry, C.D., 1997, Recent progress in understanding caldera development and mineralization in the southern Toiyama range near Round Mountain, Nevada, in Margolis, J., ed., *Low-sulfidation volcanic-hosted epithermal gold-silver deposits of west-central Nevada*: Geological Society of Nevada Special Publication 26, p. 241–246.
- Henry, C.D., Faulds, J.E., Garside, L.J., and Hinz, N.H., 2003, Tectonic implications of ash-flow tuffs in paleovalleys in the Western US: Geological Society of America Abstracts with Programs, v. 35, no. 6, p. 346.
- Hinz, N.H., Faulds, J.E., and Henry, C.D., 2003, Dextral displacement on the Honey Lake fault zone, northern Walker Lane, northeast California and westernmost Nevada: preliminary constraints inferred from Oligocene ash-flow tuff stratigraphy: Geological Society of America Abstracts with Programs, v. 35, no. 6, p. 347.
- Horton, T.W., Sjostrom, D.J., Abruzzese, M.J., Poage, M.A., Waldbauer, J.R., Hren, M., Wooden, J., and Chamberlain, C.P., 2004, Spatial and temporal variation of Cenozoic surface elevation in the Great Basin and Sierra Nevada: *American Journal of Science*, v. 304, p. 862–888, doi: 10.2475/ajs.304.10.862.
- House, M.A., Wernicke, B.P., and Farley, K.A., 1998, Dating topography of the Sierra Nevada, California, using apatite (U-Th)/He ages: *Nature*, v. 396, p. 66–69, doi: 10.1038/23926.
- House, M.A., Wernicke, B.P., and Farley, K.A., 2001, Paleogeomorphology of the Sierra Nevada, California, from

- (U-Th)/He ages in apatite: *American Journal of Science*, v. 301, p. 77–102, doi: 10.2475/ajs.301.2.77.
- Huber, N.K., 1981, Amount and timing of late Cenozoic uplift and tilt of the central Sierra Nevada, California—Evidence from the upper San Joaquin River basin, United States Geological Survey Professional Paper, Volume 1197, United States Geological Survey, p. 28.
- Huber, N.K., 1990, The late Cenozoic evolution of the Tuolumne River, central Sierra Nevada, California: *Geological Society of America Bulletin*, v. 102, p. 102–115, doi: 10.1130/0016-7606(1990)102<0102:TLCEOT>2.3.CO;2.
- Humphreys, E.D., 1995, Post-Laramide removal of the Farallon slab, western United States: *Geology*, v. 23, p. 987–990, doi: 10.1130/0091-7613(1995)023<0987:PLROTF>2.3.CO;2.
- John, D.A., Garside, L.J., and Wallace, A.R., 1999, Magmatic and tectonic setting of late Cenozoic epithermal gold-silver deposits in northern Nevada, with an emphasis on the Pah Rah and Virginia ranges and the northern Nevada Rift, in Kizis, J.A., ed., *Low-sulfidation gold deposits in northern Nevada; Olinghouse Deposit, Mule Canyon Deposit, Midas Deposit*: Geological Society of Nevada Special Publication 29, p. 65–158.
- Jones, C.H., Farmer, G.L., and Unruh, J.R., 2004, Tectonics of Pliocene removal of lithosphere of the Sierra Nevada, California: *Geological Society of America Bulletin*, v. 116, p. 1408–1422, doi: 10.1130/B25397.1.
- Kano, K., 1989, Interactions between andesitic magma and poorly consolidated sediments: Examples in the Neogene Shirahama Group, south Izu, Japan: *Journal of Volcanology and Geothermal Research*, v. 37, p. 59–75, doi: 10.1016/0377-0273(89)90113-3.
- Kano, K., 1991, Miocene pillowed sills in the Shimane Peninsula, SW Japan: *Journal of Volcanology and Geothermal Research*, v. 48, p. 359–366, doi: 10.1016/0377-0273(91)90051-Z.
- Kano, K., 1998, Explosion of volcanoclastic sediments by andesite dike intrusion: Cape Town, South Africa, *International Association of Volcanology and Chemistry of the Earth's Interior International Volcanology Congress Proceedings*, p. 29.
- Kano, K., 2002, Middle Miocene volcanoclastic dikes at Kakedo, Shimane Peninsula, SW Japan: Fluidization of volcanoclastic beds by emplacement of synvolcanic andesitic dikes: *Journal of Volcanology and Geothermal Research*, v. 114, p. 81–94, doi: 10.1016/S0377-0273(01)00283-9.
- Kokelaar, P., 1982, Fluidization of wet sediments during emplacement and cooling of various igneous bodies: *Geological Society [London] Journal*, v. 139, p. 1–17.
- Le Pourhiet, L., Gurnis, M., and Saleeby, J., 2006, Mantle instability beneath the Sierra Nevada Mountains and Death Valley extension (California, USA): *Earth and Planetary Science Letters*, v. 251, p. 104–119.
- Lindgren, W., 1911, *The Tertiary gravels of the Sierra Nevada of California*: Washington, D.C., U.S. Geological Survey, 222 p.
- Manley, C.R., Glazner, A.F., and Farmer, G.L., 2000, Timing of volcanism in the Sierra Nevada of California: Evidence for Pliocene delamination of the batholithic root?: *Geology*, v. 28, p. 811–814, doi: 10.1130/0091-7613(2000)28<811:TOVITS>2.0.CO;2.
- McKee, E.H., and Noble, D.C., 1976, Age of the Cardenas Lavas, Grand Canyon, Arizona: *Geological Society of America Bulletin*, v. 87, p. 1188–1190, doi: 10.1130/0016-7606(1976)87<1188:AOTCLG>2.0.CO;2.
- Miyabuchi, Y., 1999, Deposits associated with the 1990–1995 eruption of Unzen volcano, Japan: *Journal of Volcanology and Geothermal Research*, v. 89, p. 139–158, doi: 10.1016/S0377-0273(98)00129-2.
- Morton, J.L., Silberman, M.L., Bonham, H.F., Garside, L.J., and Noble, D.C., 1977, K-Ar ages of volcanic rocks, plutonic rocks, and ore deposits in Nevada and eastern California—Determinations run under the USGS-NBMG cooperative program: *Isocron/West*, v. 20, p. 19–29.
- Noble, D.C., Slemmons, D.B., Korrington, M.K., Dickinson, W.R., Al-Rawi, Y., and McKee, E.H., 1974, Eureka Valley Tuff, east-central California and adjacent Nevada: *Geology*, v. 2, p. 139–142.
- Oldow, J.S., 2000, Displacement transfer and differential block motion in the central Walker Lane, western Great Basin: *Eos (Transactions, American Geophysical Union)*, v. 81, p. 1174.
- Pekar, S.F., Christie-Blick, N., Miller, K.G., and Kominz, M.A., 2003, Quantitative constraints on the origin of stratigraphic architecture at passive continental margins: Oligocene sedimentation in New Jersey, U.S.A.: *Journal of Sedimentary Research*, v. 72, p. 227–245.
- Piper, A.M., Gale, H.S., Thomas, H.E., and Robinson, T.W., 1939, *Geology and ground water hydrology of the Mokelumne area, California*: U.S. Geological Survey Water-Supply Paper, v. 780, p. 230.
- Poage, M.A., and Chamberlain, C.P., 2002, Stable isotopic evidence for a pre-middle Miocene rain shadow in the western Basin and Range; implications for the paleotopography of the Sierra Nevada: *Tectonics*, v. 21, 1034, doi: 10.1029/2001TC001303.
- Proffett, J.M., Jr., and Proffett, B.H., 1976, Stratigraphy of the Tertiary ash-flow tuffs in the Yerington district, Nevada, Nevada, Bureau of Mines, Report 27, p. 28.
- Ransome, F.L., 1898, Some lava flows on the western slope of the Sierra Nevada, California: *U.S. Geological Survey Bulletin*, v. 89, p. 71.
- Roulet, F., 2006, The Miocene Dixie Mountain Volcanic Center, northern Sierra Nevada: Eroded stratovolcano or polygenetic cryptodome complex? [M.S. thesis]: Santa Barbara, University of California, 67p.
- Roulet, F.S., Busby, C.J., and Anonymous, 2005, The late Miocene Dixie Mountain volcanic center, northern Sierra Nevada; eroded stratovolcano or laccolithic intrusion?: *Geological Society of America Abstracts with Programs*, v. 37, no. 6, p. 65.
- Saleeby, J.B., and Foster, Z., 2004, Topographic response to mantle lithosphere removal in the southern Sierra Nevada region, California: *Geology*, v. 32, p. 245–248, doi: 10.1130/G19958.1.
- Saucedo, G.J., and Wagner, D.L., 1992, *Geologic Map of the Chico Quadrangle, California, 1:250,000, Regional Geologic Map Series No. 7A*: Sacramento, California, California Division of Mines and Geology.
- Schweickert, R.A., Lahren, M.M., Smith, K.D., Howle, J.F., and Ichinose, G., 2004, Transtensional deformation in the Lake Tahoe region, California and Nevada, USA: *Tectonophysics*, v. 392, p. 303–323, doi: 10.1016/j.tecto.2004.04.019.
- Sigurdsson, H., Houghton, B.F., McNutt, S.R., Rymer, H., and Stix, J., 2000, *Encyclopedia of volcanoes*: San Diego, California, Academic Press, 1471 p.
- Skilling, I.P., White, J.D.L., and McPhie, J., 2002, Peperite: A review of magma-sediment mingling: *Journal of Volcanology and Geothermal Research*, v. 114, p. 1–17, doi: 10.1016/S0377-0273(01)00278-5.
- Skilling, I., Busby, C.J., and Imai, T., 2004, Andesitic peperite-bearing debris flows; physical volcanology and paleoenvironment of the Miocene Mehrten Formation, California: *Geological Society of America Abstracts with Programs*, v. 36, no. 4, p. 85.
- Slemmons, D.B., 1953, *Geology of the Sonora Pass region* [Ph.D. thesis]: Berkeley, University of California, 222 p.
- Slemmons, D.B., 1966, Cenozoic volcanism of the central Sierra Nevada, California, geology of northern California: California Division of Mines and Geology Bulletin, v. 170, p. 199–208.
- Smith, G.A., 1991, Facies sequences and geometries in continental volcanoclastic sediments, in Fisher, R.V., and Smith, G.A., eds., *Sedimentation in volcanic settings: SEPM (Society for Sedimentary Geology) Special Publication 45*, p. 109–122.
- Snyder, G.L., and Fraser, G.D., 1963, *Pillow lavas I: Intrusive layered lava pods and pillowed lavas, Unalaska Island, Alaska*: U.S. Geological Society Professional Paper, v. 454-B, p. 1–23.
- Stock, G.M., Anderson, R.S., and Finkel, R.C., 2004, Pace of landscape evolution in the Sierra Nevada, California, revealed by cosmogenic dating of cave sediments: *Geology*, v. 32, p. 193–196, doi: 10.1130/G20197.1.
- Thatcher, W., Foulger, G.R., Julian, B.R., Svarc, J.L., Quilty, E., and Bawden, G.W., 1999, Present-day deformation across the Basin and Range Province, western United States: *Science*, v. 283, p. 1714–1718, doi: 10.1126/science.283.5408.1714.
- Trexler, J.H., Jr., Cashman, P.H., Muntean, T., Schwartz, K., Ten Brink, A., Faulds, J.E., Perkins, M., and Kelly, T., 2000, Neogene basins in western Nevada document the tectonic history of the Sierra Nevada—Basin and Range transition zone for the last 12 Ma, in Lageson, D.R., et al., eds., *Great Basin and Sierra Nevada: Geological Society of America Field Guide*, v. 2, p. 97–116.
- Unruh, J.R., 1991, The uplift of the Sierra Nevada and implications for late Cenozoic epeirogeny in the western Cordillera: *Geological Society of America Bulletin*, v. 103, p. 1395–1404, doi: 10.1130/0016-7606(1991)103<1395:TUOTSN>2.3.CO;2.
- Unruh, J.R., Humphrey, J., and Barron, A., 2003, Transtensional model for the Sierra Nevada frontal fault system, eastern California: *Geology*, v. 31, p. 327–330, doi: 10.1130/0091-7613(2003)031<0327:TMFTSN>2.0.CO;2.
- Voigt, B., Constantine, E.K., Siswoidjyo, S., and Torley, R., 2000, Historical eruptions of Merapi Volcano, Central Java, Indonesia, 1768–1998: *Journal of Volcanology and Geothermal Research*, v. 100, p. 69–138, doi: 10.1016/S0377-0273(00)00134-7.
- Wagner, D.L., and Saucedo, G.J., 1990, Age and stratigraphic relationships of Miocene volcanic rocks along the eastern margin of the Sacramento Valley, California, in Ingersoll, R.V., and Nilsen, T.H., eds., *Sacramento Valley Symposium Guidebook, Volume 65: Pacific Section, SEPM (Society for Sedimentary Geology)*, p. 143–151.
- Wagner, D.L., Jennings, C.W., Bedrossian, T.L., and Fortugno, E.J., 1981, *Geologic Map of the Sacramento Quadrangle 1:250,000, Regional Geologic Map Series, Map no. 1A*, California Division of Mines and Geology.
- Wagner, D.L., Saucedo, G.J., and Grose, T.L.T., 2000, Tertiary Volcanic Rocks of the Blairsden Area, Northern Sierra Nevada, California, in Brooks, E.R., and Dida, L.T., eds., *Field Guide—Geology and Tectonics of the Northern Sierra Nevada: National Association of Geoscience Teachers Far-Western Section Fall Conference, 2000, Volume 122*, California Division of Mines and Geology Special Publication, p. 155–172.
- Wakabayashi, J., and Sawyer, T.L., 2001, Stream incision, tectonics, uplift, and evolution of topography of the Sierra Nevada, California: *Journal of Geology*, v. 109, p. 539–562, doi: 10.1086/321962.
- Wernicke, B., 1992, Cenozoic extensional tectonics of the U.S. Cordillera, in Burchfield, B.C., et al., eds., *The Cordilleran orogen: Conterminous U.S.: Boulder, Colorado, Geological Society of America, Geology of North America*, v. G-3, p. 553–581.
- Whitney, J.D., 1880, *The Auriferous Gravels of the Sierra Nevada of California*, Contributions to American Geology: Memoirs of the Museum of Comparative Zoology, Volume 1: Cambridge, Massachusetts, Harvard University Press, 659 p.
- Williams, H., 1929, *Geology of the Marysville Buttes, California*: University of California Publications in Geological Sciences, v. 18, p. 103–120.
- Williams, H., and Curtis, G.H., 1977, *The Sutter Buttes of California: A study of Plio-Pleistocene volcanism*: University of California Publications in Geological Sciences, v. 116, p. 56.
- Wolfe, J.A., Schorn, H.E., Forest, C.E., and Molnar, P., 1997, Paleobotanical evidence for high altitudes in Nevada during the Miocene: *Science*, v. 276, p. 1672–1675, doi: 10.1126/science.276.5319.1672.

MANUSCRIPT RECEIVED 1 JUNE 2005
 REVISED MANUSCRIPT RECEIVED 21 MARCH 2007
 MANUSCRIPT ACCEPTED 23 MARCH 2007

Printed in the USA